Water Research 264 (2024) 122130

Contents lists available at ScienceDirect

Water Research

journal homepage: www.elsevier.com/locate/watres

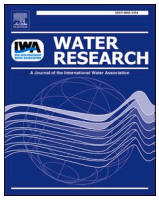

Linking pattern shifts of dissolved organic nitrogen fractional removal with microbial species richness in a cascade upflow biofiltration process

Alejandra Robles-Lecompte [a], Jinxiang Cheng [a], Amy M. McKenna [b,c], Ni-Bin Chang [a,*]

[a] Department of Civil, Environmental, and Construction Engineering, University of Central Florida, Orlando, FL, USA
[b] National High Magnetic Field Laboratory, Florida State University, Tallahassee, FL, USA
[c] Department of Soil and Crop Sciences, Colorado State University, Fort Collins, CO, USA

ARTICLE INFO

Keywords:
Dissolved organic nitrogen
21 tesla
Dissolved organic matter
Fourier transform ion cyclotron resonance mass spectrometry
Quantitative polymerase chain reaction
Nitrate removal

ABSTRACT

Nutrient pollution has become an important issue to solve in stormwater runoff due to the fast population growth and urbanization that impacts water quality and triggers harmful algal blooms. There is an acute need to link the dissolved organic nitrogen (DON) decomposition with the coupled nitrification and denitrification pathways to realize the pattern shifts in the nitrogen cycle. This paper presented a lab-scale cascade upflow biofiltration system for comparison of nitrate and phosphate removal from stormwater matrices through two specialty adsorbents at three influent conditions. The two specialty adsorbents are denoted as biochar iron and perlite integrated green environmental media (BIPGEM) and zero-valent iron and perlite-based green environmental media (ZIPGEM). An initial condition with stormwater runoff, a second condition with spiked nitrate, and a third condition with spiked nitrate and phosphate were used in this study. To differentiate nitrifier and denitrifier population dynamics associated with the decomposition of DON, integrative analysis of quantitative polymerase chain reaction (qPCR) and 21 tesla Fourier transform ion cyclotron resonance mass spectrometry (FT-ICR MS) were performed in association with nitrate removal efficiencies for both media with or without the presence of phosphate. While the qPCR may detect one gene for a single microbe or pathogen and realize the microbial population dynamics in the bioreactors, the 21 T FT-ICR MS can separate and assign elemental compositions to identify organic compounds of DON. Results indicated that ZIPGEM obtained a higher potential for nutrient removal than BIPGEM when the influent was spiked with nitrate and phosphate simultaneously. The sustainable, scalable, and adaptable upflow bioreactors operated in sequence (in a cascade mode) can be expanded flexibly on an as-needed basis to meet the local water quality standards showing process reliability, resilience, and sustainability simultaneously.

1. Introduction

Nutrient pollution, especially nitrogen and phosphorus, has increasingly become an issue in stormwater treatment (Valencia et al., 2020). Nitrogen can be present in stormwater runoff as organic or inorganic nitrogen. Inorganic nitrogen exists in ammonia (NH_3) / ammonium (NH_4^+), nitrate (NO_3^-), nitrite (NO_2), nitric oxide (NO), nitrous oxide (N_2O^-), and nitrogen gas (N_2), and dissolved organic nitrogen (DON) is any subset of dissolved organic matter (DOM) that contains nitrogen (Miranda et al., 2023), such as proteins (Madigan et al., 2021), urea (Zhang et al., 2021), dissolved combined amino acids, dissolved free amino acids, humic and fulvic substances, and nucleic acids (Berman and Bronk, 2003). Removal of inorganic nitrogen in an engineered process or a natural environment was performed via the biochemical mechanism, such as nitrification, denitrification, nitrogen fixation, ammonification, and dissimilatory nitrate reduction (Valencia et al., 2020). However, the key to success is how fast the decomposition of DON can occur to trigger ammonification and how sensitive the downstream population of nitrifiers and denitrifiers can respond to the upstream DON decomposition to complete the prescribed role in the nitrogen cycle. This part of the science has not yet been well addressed due to the missing link between pattern shifts of DON fractional removal with microbial species richness for nitrification and denitrification.

When excessive amounts of inorganic nitrogen and DON become harmful to stormwater runoff, it is important to treat the surface water with cost-effective, scalable, adaptable, and sustainable environmental

* Corresponding author.
E-mail address: nibinchang@gmail.com (N.-B. Chang).

https://doi.org/10.1016/j.watres.2024.122130
Received 15 November 2023; Received in revised form 16 July 2024; Accepted 20 July 2024
Available online 26 July 2024

Location	Description	Location	Description
1	Effluent of water pump	5	Top of gravel for upstream bioreactor
2	Initial Reservoir	6	Feed reservoir of downstream bioreactor
3	Effluent ports of initial reservoir	7	Top of gravel for downstream bioreactor
4	Feed reservoir of upstream bioreactor	8	Effluent of downstream bioreactor

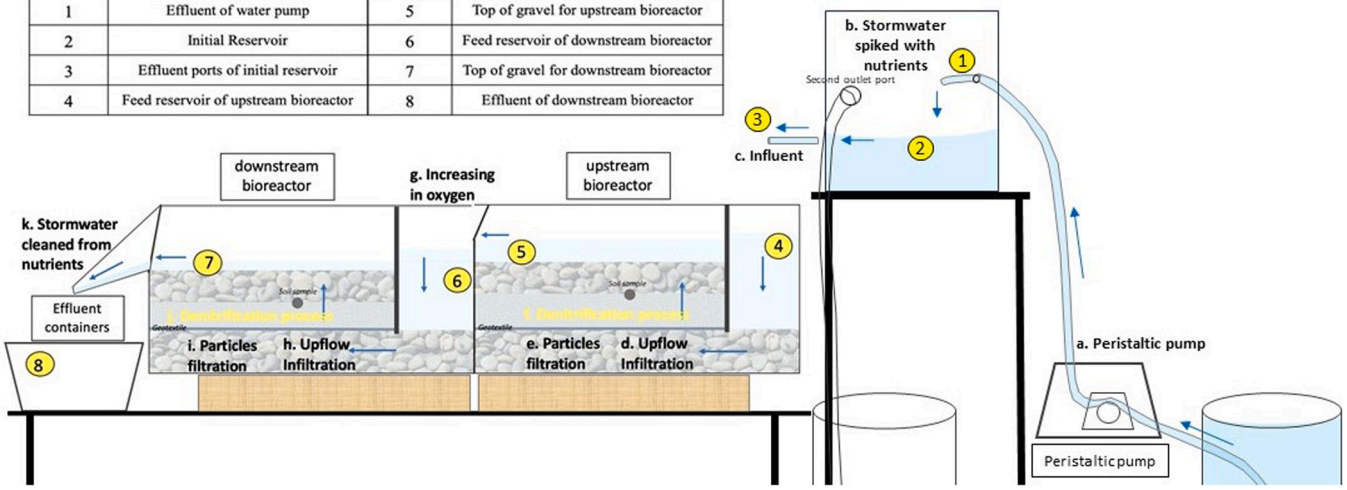

Fig. 1. Process schematic of the cascade upflow biofiltration systems.

technologies (Chang et al., 2010; Chang et al., 2018b; Crites and Tchobanoglous, 1998; Valencia et al., 2020; Wen et al., 2020b). Many filtration systems use vertical sand-based filtration, which has some problems associated with clogging (Kilgus-Vesely, 2023; Lahin et al., 2021), flooding, and settlement (Cooper, 2005). However, media clogging and flooding problems may be resolved by changing flow direction from downflow to uplfow. Although DON decomposition is significant in nitrogen removal, few earlier studies have touched upon the ammonification effect of DON in nitrogen removal while more emphasis was placed on the nitrification and denitrification (Libby and Wheeler, 1997; Hansell and Waterhouse, 1997; Raimbault et al., 1999). Previous studies explored the phenomenon when DON concentration increases and nitrate pollution decreases. Although DON can be linked with nitrate amounts, there are some cases when DON concentrations do not correlate directly with a decrease in nitrate (Berman and Bronk, 2003). According to Wen et al. (2019), DON is a structurally complex mixture of four major classes of biological macromolecules (i.e., lipids-like, proteins, carbohydrates-like, and nucleic acids) in term of chemical structure and composition that involve various microorganism during DON decomposition. The growth of these microorganism species depends on environmental conditions, biogeochemical processes, the type of filter media, and water conditions (i.e., temperature, pH, dissolved oxygen, light abundance, media morphology, structure, and texture, and nutrients abundance; Madigan et al., 2021).

Biochar and zero-valent iron (ZVI) have received significant attention as low-cost, low-impact adsorbents for the removal of heavy metals, pathogens, and nutrients due to their ability to aid in structural support and reasonable removal efficiencies in green sorption media (GSM; Gopal et al., 2020; Plessl et al., 2023; Tian et al., 2023; Wen et al., 2020a; Zheng et al., 2023; Zhu et al., 2020). GSM-based filtration technology has been developed to treat nutrient pollution in stormwater runoff (Valencia et al., 2020), wastewater effluent (Chang et al., 2010), and agriculture discharge (Wen et al., 2019). Engineered GSM as specialty adsorbents are aimed to remove nitrate and phosphate via physiochemical and microbiological processes simultaneously. The use of GSM may lead to the balance among media characteristics, hydraulic loading rates, and physiochemical and microbiological reactions to achieve process reliability, sustainability, and resilience (Wen et al., 2018; Chang et al., 2019). Yet there is still a need to bridge the knowledge gap between the DON decomposition toward ammonification and the coupled nitrification and denitrification process in a biofiltration system composed of new GSM via an integrative analysis.

This study explored such a key challenge for linking pattern shifts of DON fractional removal with microbial species richness in a cascade upflow biofiltration system for nitrate and phosphate removal. It uniquely addressed how DON decomposition occurred in two distinct media in connection to downstream nitrification and denitrification. The two distinct GSM are biochar-based iron and perlite integrated green environmental media (BIPGEM) and ZVI and perlite-based green environmental media (ZIPGEM). These filtration media mixtures contain natural and recycled materials such as iron, aluminum, calcium, potassium, and carbon filings (only in BIPGEM) that work as macro and micronutrient sources for microorganisms to grow. The integrative analysis is aimed at linking the DON decomposition with the coupled nitrification and denitrification pathways via an integrative analysis of quantitative polymerase chain reaction (qPCR) and Fourier transform ion cyclotron resonance mass spectrometry (FT-ICR MS). qPCR may help explore two oxidation reactions in which ammonia (NH_3) / ammonium (NH_4^+) is catalyzed by ammonia oxidizing bacteria-AOB (amoA) to become nitrite (NO_2^-). Consecutively, nitrite (NO_2^-) is catalyzed by nitrate oxidizing bacteria-NOB (nxrAB) to produce nitrate (NO_3^-; Madigan et al., 2021; Valencia et al., 2020). Moreover, the denitrification pathway promotes reduction reactions where all denitrifying bacteria, such as narG, nirS, norB, and nosZ, reduce the oxygen from nitrate (NO_3^-) to nitrite (NO_2^-), nitric oxide (NO), nitrous oxide (N_2O^-), and nitrogen gas (N_2), respectively (Chang et al., 2010; van Spanning et al., 2007; Ehrlich and Newman, 2008). FT-ICR MS may investigate the DON fractional removal with respect to lipids, proteins/amino sugars, lignins, tannins, condensed aromatics, and carbohydrates. These steps during the DON fractional removal represent the metabolic pathways catalyzed by specific bacteria in DON mineralization and/or photoammonification (Liu et al., 2016; Shrestha et al., 2018; Yang et al., 2021; van Spanning et al., 2007).

The objective of this study was thus to compare the microbiological processes of two GSM for nutrient removal in stormwater runoff via an upflow reactor to increase the hydraulic loading and avoid the possible clogging issue in downflow reactors. Moreover, an integrative analysis of qPCR and negative-ion electrospray ionization 21 T FT-ICR MS was performed to deepen our understanding of the relationship between microbial communities and metabolic pathways related to DON compounds of two upflow bioreactors composed of BIPGEM and ZIPGEM, respectively, at different influent conditions. This led to linking the relative abundance of DON in each different heteroatom class with the population density of nitrifying (AOB and NOB) and denitrifying bacteria (nirS and nosZ). The research questions to be answered include the following: (1) Can the presence of biochar promote the growth of denitrifiers in the upflow biofiltration system? (2) Does the presence of nitrate and phosphate affect the relative abundance of DON across the

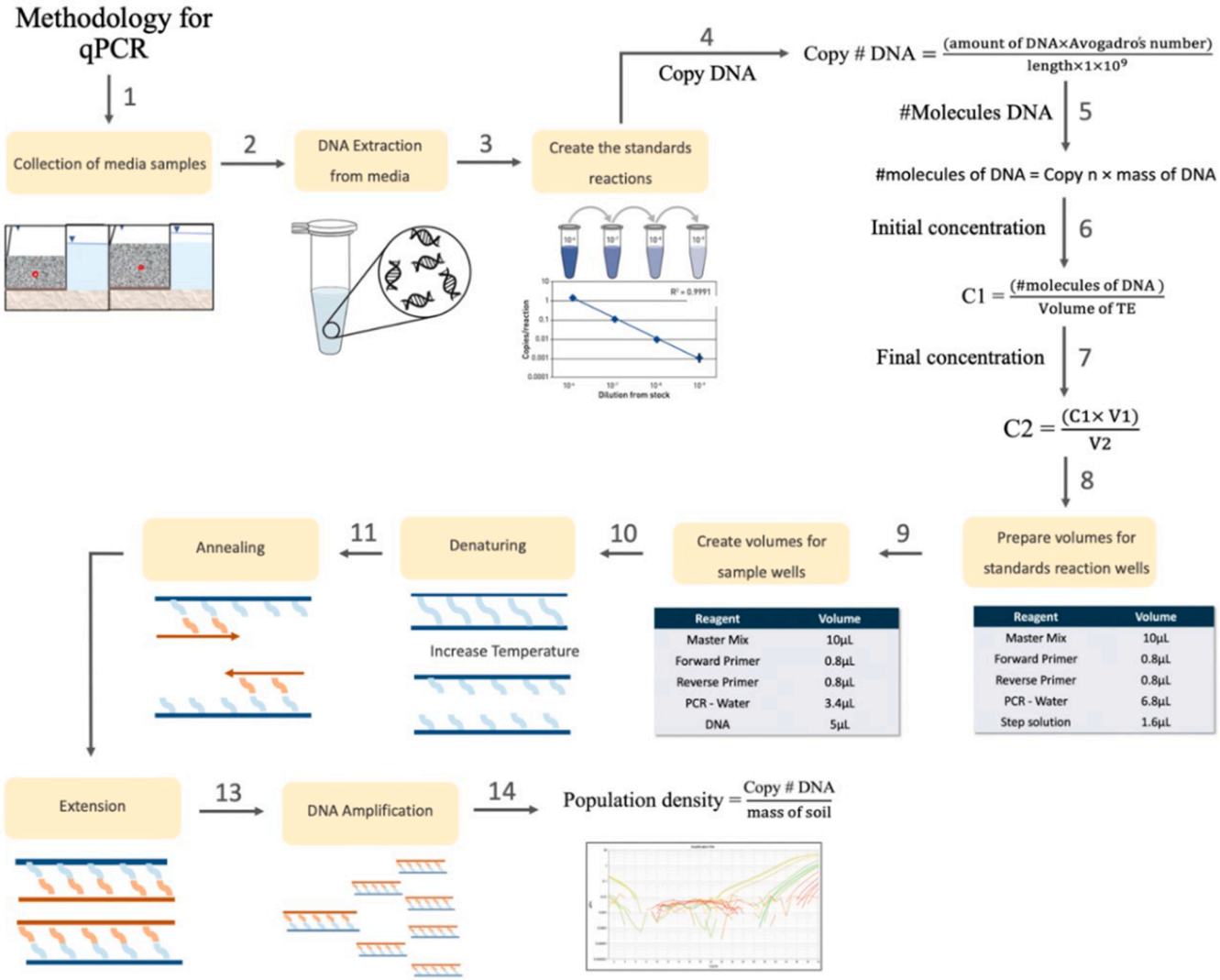

Fig. 2. The analytical process of qPCR in detail. (1) Collection of samples. (2) DNA extraction from the media. (3) Creation of standards reactions. (4) Equation of DNA copy. (5) Equation of molecules of DNA. (6) Initial concentration. (7) Final concentration. (8) Creation of volumes for standards reactions. (9) Creation of volumes per sample well. (10) Denaturing process. (11) Annealing process. (12) Extension process. (13) DNA amplification. (14) Population density equation.

bioreactors? We hypothesize the following: (1) The presence of biochar in BIPGEM increases higher population density of nirS and nosZ genes compared with ZIPGEM; (2) the presence of nitrate and phosphate in the influent of the bioreactors increases the relative abundance of DON for complex molecules that contain N4 heteroatom class.

2. Material and methods

2.1. Experimental design and operation

To create a sustainable, adaptable, and scalable water treatment system in local drainage landscape, two upflow biofiltration systems in parallel, each containing a different media recipe, were thus constructed to run for a 3-week incubation in 2023. Each system tested either BIPGEM or ZIPGEM in two bioreactors operated in sequence (i.e., in a cascade mode) and more bioreactors in a cascade mode can be added into each biofiltration system on an as-needed basis to meet the local water quality standards. BIPGEM was composed of 80 % Sand, 5 % Clay, 5 % ZVI, 5 % Perlite, and 5 % Biochar, and ZIPGEM contained 85 % Sand, 5 % Clay, 5 % ZVI, and 5 % Perlite (Ordonez et al., 2022). The bioreactor setup was made up of a peristaltic pump, one initial reservoir tank as the influent (location 2 in Fig. 1), an upstream bioreactor (location 5 in Fig. 1), a downstream bioreactor (location 7 in Fig. 1), and an effluent container (location 8 in Fig. 1). Stormwater runoff from a wet detention pond beside the Student Union Building at UCF was collected to run the bioreactors. The stormwater ran through the peristaltic pump to keep a steady flow rate in the influent ports. The upstream bioreactor included two compartments: (1) the feed reservoir to store the water with dimensions of $3 \times 8 \times 13\ cm^3$ (length, width, height); (2) the media reservoir, which was composed of gravel at the bottom (1.3 cm height) and overlaid by a geotextile, media (either 3 cm in height of ZIPGEM or BIPGEM), and 1.5 cm of a layer of gravel on top to prevent the media from suspension (Fig. 1). The downstream bioreactor followed the same layout as the upstream bioreactor but with different dimensions for the media reservoir (only 2 cm in height of ZIPGEM or BIPGEM). Staggered triangular channels connected the bioreactors to generate a cascade effect.

Following such understanding, the experimental design consisted of three distinct stages: (1) a physicochemical process stage, as evidenced by low values of oxide-reduction potential (ORP) during the first two 2 weeks; (2) an incubation stage, which showed low nitrate removal efficiencies and about 150 millivolts of ORP values during following 3 weeks; and (3) a microbiological stage, where the nitrate concentrations of stormwater runoff were spiked and nitrate removal efficiencies and

Table 1
Target genes, primers, sequences associated, and thermocycling.

Name of Bacteria	Genes	Primer's name	Sequence	Thermocycling	Reference
AOB	amoA	amoA1F amoA2R	GGGGTTTCTACTGGTGGT CCCCTKGSAAAGCCTTCTTC	50 °C for 2 min, 95 °C for 2 min holding stage, 45 cycles at 95 °C for 15 s, and 62 °C for 1 min	Rotthauwe et al., 1997
NOB	nxrAB	NSR 113F NSR1264R	CCTGCTTTCAGTTGCTACCG GTTTGCAGCGCTTTGTACCG	50 °C for 2 min, 95 °C for 2 min holding stage, 45 cycles at 95 °C for 15 s, and 62 °C for 1 min	Dionisi et al., 2002
Denitrifiers	nirS	Cd3AF R3Cd	GTSAACGTSAAGGARACSGG GASTTCGGRTGSGTCTTGA	50 °C for 2 min, 95 °C for 10 min holding stage, 40 cycles at 95 °C for 60 s, 51 °C for 60 s, and 60 °C for 1 min	Azziz et al., 2017
	nosZ	nosZ-F nosZ1622R	CGYTGTTCMTCGACAGCCAG CGSACCTTSTTGCCSTYGCG	94 °C for 2 min, 35 cycles at 94 °C for 30 s, 57 °C for 40 s, and 72 °C for 40 s	Kloos et al., 2001

the corresponding ORP values increased. Before stage 3, bioreactors ran with stormwater runoff with their natural nutrient concentrations (or without spiking), which was referred to as "before condition 1″ (BC1). During stage 3, the stormwater runoff was spiked with 1.5 mg•L^{-1} of nitrate for 2.5 h for both bioreactors, which was referred to as "after condition 1″ (AC1). Then, the stormwater runoff was spiked with 1.5 mg•L^{-1} of nitrate and 1.0 mg•L^{-1} of phosphate for 2.5 h for both bioreactors to create the last influent condition during stage 3, which was referred to as "after condition 2″ (AC2). Hydraulic data and water quality parameters were collected during the three distinct stages from BC1 to AC2. The flow rate (Q) was collected in triplicates in the influent (location 2) and effluent (location 8) to control steady state system across the bioreactors. These results were measured by collecting volume of water during specific time (ml•min^{-1}). Simultaneously, ORP, dissolved oxygen (DO), and pH values were measured at the same locations over the experimental timeframe with a Milwaukee PRO ORP meter, HACH HQ40d DO meter, and Pmoyoko pH meter, respectively.

2.2. Quantitative polymerase chain reaction

The qPCR analysis procedure was performed to explore the microbial population dynamics by same method developed by Chang et al. (2018b). This process included the following steps: (1) collection of media samples; (2) DNA extraction; (3) preparing standard reactions and volumes; (4) denaturing; (5) annealing; (6) elongation; and (7) DNA amplification (Fig. 2). After one month of incubation, a set of 1-gram media samples was collected from the top of each bioreactor at the three different conditions. Then, DNA was extracted from the collected media samples with a DNeasy PowerSoil Kit with Powerbead tubes, Solutions C1 to C5, MB Spin Columns, and 2 mL collection tubes (Valencia et al., 2020; Wen et al., 2019). Ammonia oxidizing bacteria (AOB), nitrite oxidizing bacteria (NOB), and denitrifying genes (nirS and nosZ) were the four target genes used to conduct the qPCR (Table 1). Fig. 2 depicted the different equations applied to assay standards. The setup plate per each analyzed sample included five assays for standards, a triplicated DNA sample, and one negative well. First, the copy number

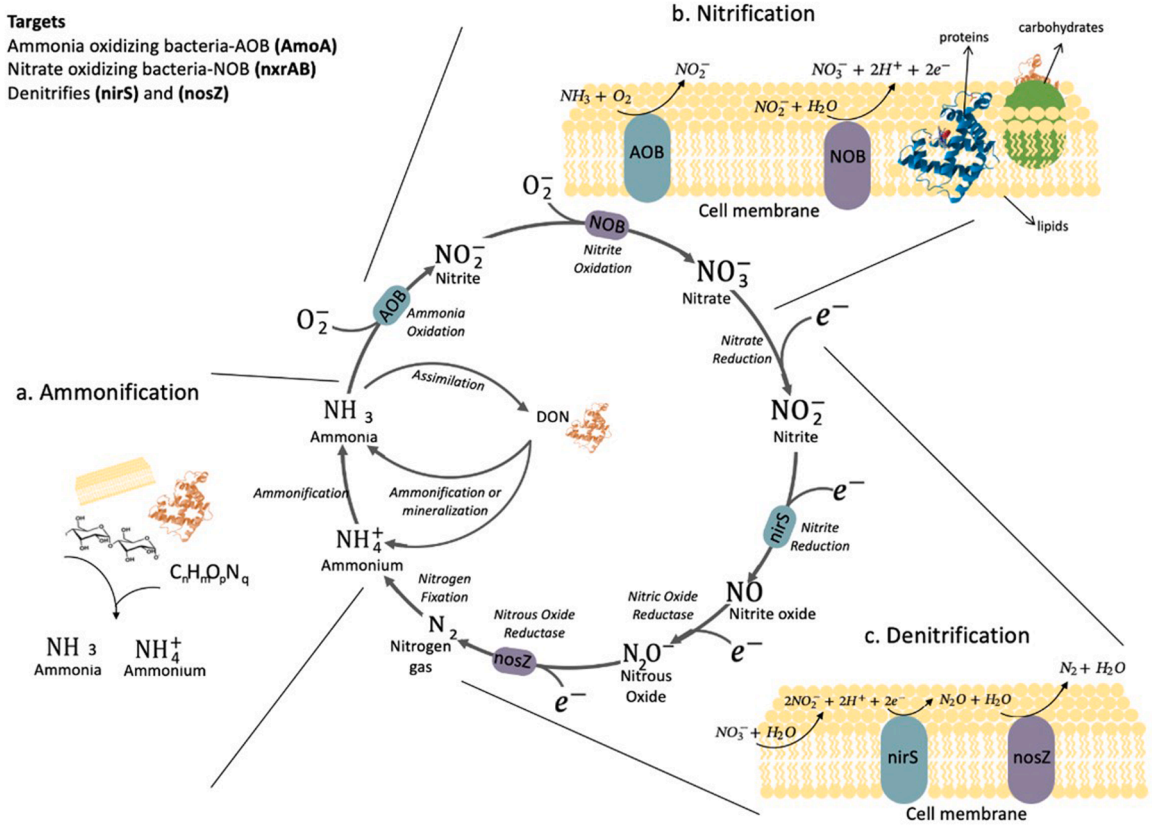

Fig. 3. (a) Nitrogen cycle. (b) Nitrification pathway via ammonia oxidizing bacteria and nitrate oxidizing bacteria. (c) Denitrification pathway including nitrite reduction and nitrous oxide reductase (nirS and nosZ). Microbial population density across the bioreactors. Edited from Chang et al., 2010; Valencia et al., 2020; Wen et al., 2020b; Madigan et al., 2021.

of the DNA (mol) was calculated in Eq. (1) based on the length of each target, and the conversion to #molecule was represented in Eq. (2), where the amount of DNA = nanograms of DNA (ng), Avogadro's number = the conversion factor (molecules·mol^{-1}), and length = base pair (bp). Second, the initial concentration (C_1) in (#molecules · μl^{-1}) or concentration in stock was calculated in Eq. (3), where Volume TE = Volume TE Buffer (µl), a substance to protect the DNA from auto-degradation (Griffiths et al., 2011). Finally, the final concentration (C_2) in (#molecules · μl^{-1}) of assay standard per well was obtained from Eq. (4), where V_1 = initial volume or stock volume (µl) and V_2 = final volume or volume of assay standard per well (µl; Biosystems, 2015). The PowerUp SYBR Green master mix was used to perform the qPCR procedure (Wen et al., 2019).

$$Copy\ \#\ DNA = \frac{(amount\ of\ DNA\ \times\ Avogadro's\ number)}{length\ \times\ 1\ \times\ 10^9} \quad (1)$$

$$\#\ molecules\ DNA = Copy\ \#\ DNA\ \times\ mass\ DNA \quad (2)$$

$$C_1 = \frac{(\#\ molecules\ DNA)}{volume\ of\ TE} \quad (3)$$

$$C_2 = \frac{(C_1\ \times\ V_1)}{V_2} \quad (4)$$

$$Population\ density = \frac{Copy\ \#\ DNA}{mass\ of\ soil} \quad (5)$$

After placing the samples in qPCR machine cycling, denaturing was carried out via a process where samples were under high temperatures to break and separate double-stranded DNA into two single strands (Chang et al., 2018b; Scientific, 2014; Fig. 2). These temperatures were different according to the sequence of each target in Table 1. After denaturing, the temperature was reduced, and primers were able to attach to the corresponding target of the single-strand DNA (Chang et al., 2018b; Scientific, 2014). The elongation time for all the primers was 95 °C for 15 s, 60 °C for 60 s, and 95 °C for 15 s, following Valencia et al. (2020). During DNA amplification, a fluorescence signal was emitted by a probe. This fluorescence signal was plotted to produce a melting curve. The results were displayed by the StepOne qPCR System where was quantified the # copy DNA (Chang et al., 2018b). Consequently, the population density of each target was calculated based on Eq. (5). With this experimental setup, it enabled us to address the DON decomposition in the (Fig. 3).

2.3. DON analysis by 21 T FT-ICR MS

2.3.1. DON sample collection

We collected five hundred mL of water samples for influent and effluent during two inlet condition runs (AC1 and AC2) for BIPGEM and ZIPGEM. Impurities were reduced by preparing samples via solid phase extraction by using a filtration process employing the Bond Elut™ PPL cartridge (200 mg, 3 mL) and methanol to elude the sorbet bed (Valencia et al., 2020). All sample extracts were delivered to the National High Magnetic Field Laboratory (NHMFL) in Tallahassee, Florida, and eluted species analyzed by negative-ion electrospray ionization FT-ICR MS at 21 tesla. All solvents were HPLC grade (Sigma-Aldrich Chemical Co., St. Louis, MO) and SPE extracts were diluted in MeOH to a final concentration of 100 ppm. For instrumentation, the sample solution was infused via a micro-electrospray source (Emmett et al., 1998; 50 µm i.d. fused silica emitter) at 500 nL·min^{-1} by a syringe pump. Typical conditions for negative ion formation were emitter voltage (−2.8 to 3.2 kV), S-lens RF level (45 %), and heated metal capillary temperature (350 °C).

2.3.2. DON instrumental analysis

DOM extracts were analyzed with a custom-built hybrid linear ion trap FT-ICR MS equipped with a 21 T superconducting solenoid magnet (Hendrickson et al., 2015). Negative ions were initially accumulated in an external multipole ion guide (1–5 ms) and released m·z^{-1} dependently by the decrease of an auxiliary radio frequency potential between the multipole rods and the end-cap electrode (Hendrickson et al., 2015; Smith et al., 2018). Ions were excited to an m·z^{-1} dependent radius to maximize the dynamic range and number of observed mass spectral peaks (32–64 %), and excitation and detection were performed on the same pair of electrodes (Kaiser et al., 2013). The dynamically harmonized ICR cell in the 21 T FT-ICR was operated with 6 V trapping potential (Chen et al., 2014). Time-domain transients of 3.1 s were conditionally co-added and acquired with the Predator data station that handled excitation and detection only, initiated by a TTL trigger from the commercial Thermo data station with 100 time-domain acquisitions averaged for all experiments (Kaiser et al., 2013; Boldin and Nikolaev, 2011). Mass spectra were phase corrected (Xian et al., 2010) and internally calibrated with 10 to 15 highly abundant oxygen homologous series that spanned the entire molecular weight distribution based on the "walking" calibration method (Savory et al., 2011).

Experimentally measured masses were converted from the International Union of Pure and Applied Chemistry mass scale to the Kendrick mass scale (Kendrick, 1963) for rapid identification of homologous series for each heteroatom class (i.e., species with the same $C_cH_hN_nO_oS_s$ content, differing only be degree of alkylation; Miranda et al., 2023). For each elemental composition, $C_cH_hN_nO_oS_s$, the heteroatom class (Hughey et al., 2001) and carbon number, c, were tabulated for subsequent generation of heteroatom class relative abundance distributions and graphical relative-abundance weighted images and van Krevelen diagrams (Krevelen, 1950). Molecular formula assignments and data visualization were performed with PetroOrg© software (Corilo, 2014; Miranda et al., 2023). All mass spectra presented herein is depicted in Table 2. The DON concentration of each heteroatom class was obtained accordingly (Chang et al., 2018a).

Table 2
Nitrogen-containing species assigned per samples.

Sample	No. peaks assigned	No. peaks with nitrogen-containing species	Root of mean square error for assignments (ppb)
BB_AC1_Influent	35,160	73	63
BB_AC1_Effluent	29,060	76	63
BZ_AC1_Influent	26,741	70	58
BZ_AC1_Effluent	26,293	72	59
BB_AC2_Influent	28,232	76	58
BB_AC2_Effluent	27,201	71	58
BZ_AC2_Influent	27,502	72	60
BZ_AC2_Effluent	27,730	70	61

2.4. Material characterization

X-ray fluorescence (XRF) was used to conduct a chemical composition analysis, and it enabled us to identify and compare different chemical elements of ZIPGEM and BIPGEM at different stages and conditions. The chemical compositions of the different media were analyzed via an XRF PANalytical Epsilion at the Advanced Materials Processing and Analysis Center at UCF (Dewi et al., 2018).

2.5. Statistical analysis

Principal component analysis (PCA) is a multivariate technique that analyzes data described by several correlated quantitative dependent variables (Mishra et al., 2017). In this study, PCA was performed to connect components that control the bioreactor conditions, such as denitrifier population density, chemical composition, hydraulic retention time (HRT), and influent nutrient concentrations with nitrate removal efficiencies. The input data for the PCA analysis included an HRT test, qPCR, and XRF. The correlation percentage of different

Table 3
Percent of chemical composition of BIPGEM and ZIPGEM associated with the BC1 and AC2 conditions via an XRF analysis.

Samples	Si (%)	Al (%)	Fe (%)	Others (%)
ZIPGEM-BC1	55.267	13.434	19.976	11.324
BIPGEM-BC1	45.559	1.096	44.080	9.265
ZIPGEM-AC2	44.468	14.416	32.758	8.358
BIPGEM-AC2	27.209	7.1315	58.584	7.076

principal components (e.g., PC1 and PC2) were obtained based on each media and experimental conditions to aid in data interpretation.

3. Results

3.1. Material composition

According to Table 3, Si is the principal element and around 55 % and 45 % exist in the BC1 media matrix of ZIPGEM and BIPGEM, respectively; however, there are much less Si elements in the AC2 media matrix of ZIPGEM and BIPGEM, around 44 % and 27 %, respectively. The second abundant element is Al, and the values in between the ZIPGEM and BIPGEM media matrix are very dissimilar. It is notable that the change of Si and Al from BC1 to AC2 is phenomenal, highlighting the impact of the physicochemical process in the initial two weeks of this experiment.

3.2. Biofiltration system

The range of ORP and nitrate removal efficiency over the three prescribed stages in the biofiltration system filled with BIPGEM and ZIPGEM are shown in Fig. 4(a) and Fig. 4(b), respectively. Stage 1 was predominated by the physicochemical process was emphasized, and ferric iron becomes ferrous iron within the range of the ORP (+100 and −100 mV) such that the nitrate removal efficiency was higher because of the removal mechanisms in the physicochemical process. Stage 2 was designed as the incubation period by feeding the stormwater collected

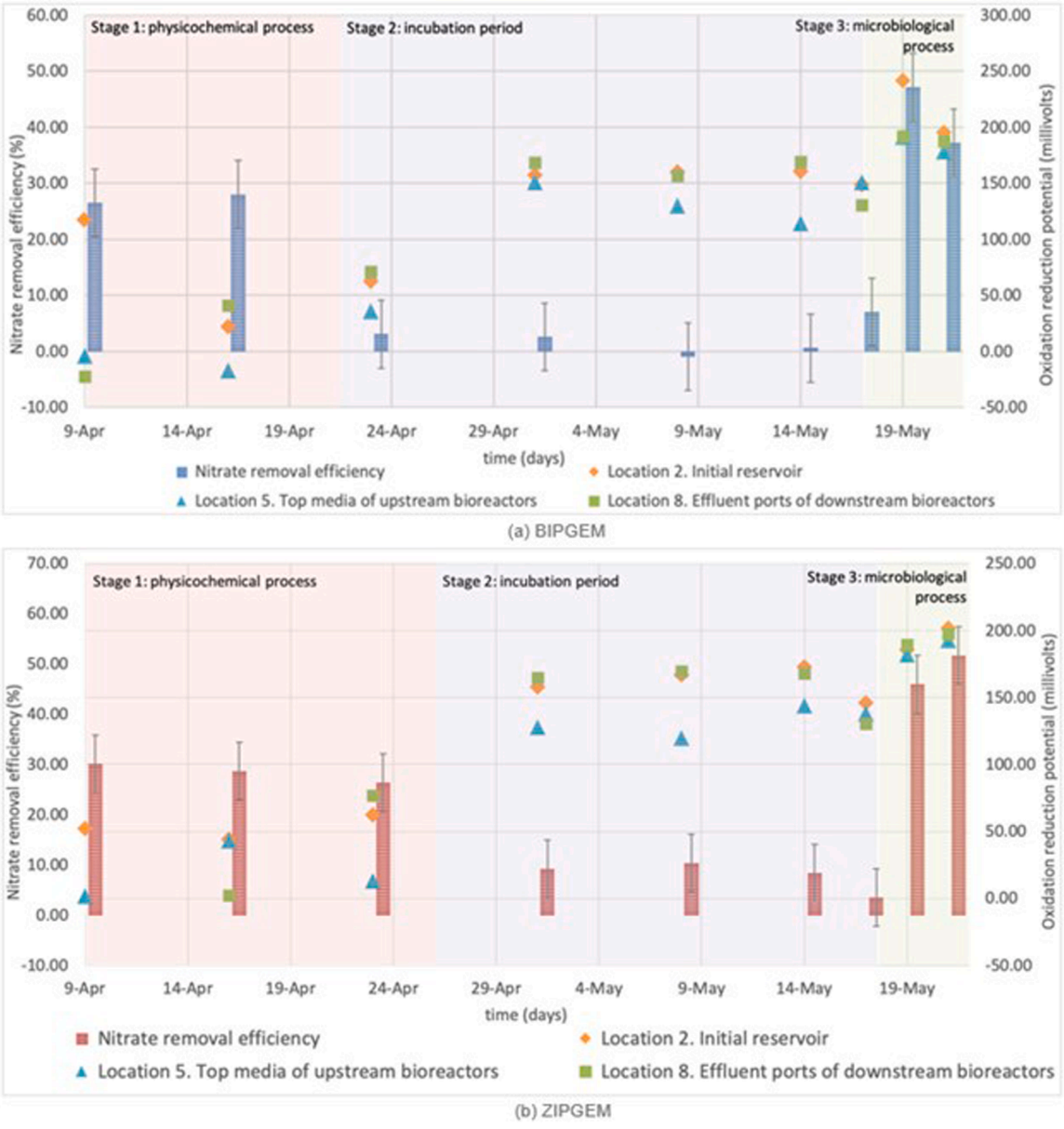

Fig. 4. Nitrate removal efficiencies (left axis) and ORP values (right axis). (a) BIPGEM; (b) ZIPGEM. Removal efficiencies (%) were represented in bars and ORP values in triangles.

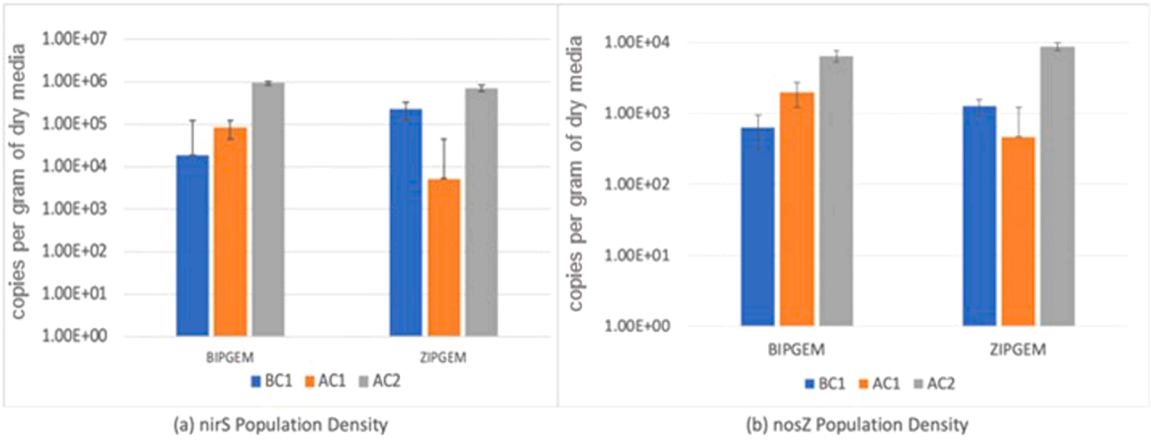

Fig. 5. (a) nirS population density for BIPGEM (left) and ZIPGEM (right) at three different influent conditions. (b) nosZ population density for BIPGEM (left) and ZIPGEM (right) at three different influent conditions.

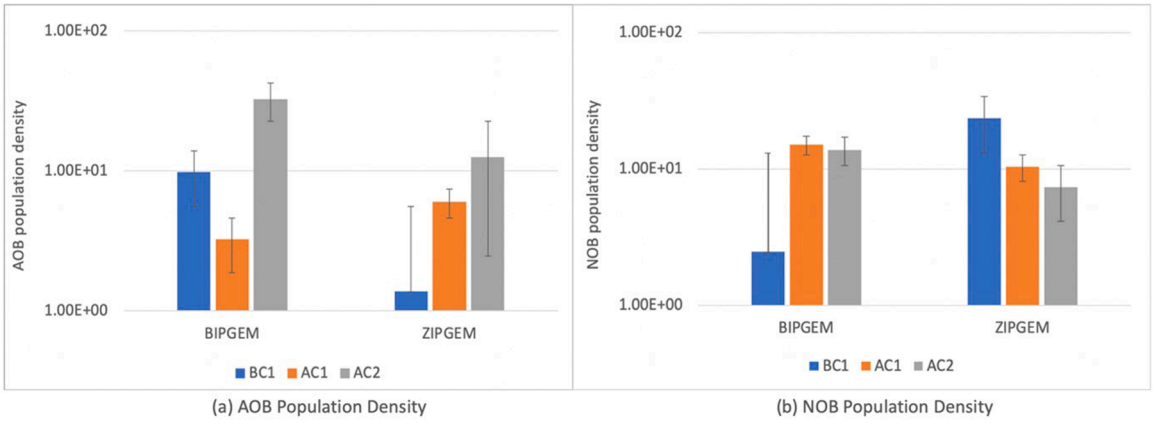

Fig. 6. (a) AOB population density for BIPGEM (left) and ZIPGEM (right) at three different influent conditions. (b) NOB population density for BIPGEM (left) and ZIPGEM (right) at three different influent conditions.

from a wet detention pond, and the ORP values increased in a range from +100 to +200 mV for both media.

However, the low nitrate removal efficiency indicated there was no presence of denitrifying microorganisms as evidenced by the qPCR results. Stage 3 was dominated by the microbiological process, and the ORP measurements and nitrate removal efficiency values increased simultaneously as also evidenced by the qPCR results. The hydraulic loading in cascade upflow biofiltration process is larger than that in downflow systems (Ordonez et al., 2020a, 2020b).

3.3. Population dynamics of microbial species

Population density of nitrogen cycle microbial ecology was analyzed via qPCR for both bioreactors (BIPGEM and ZIPGEM) at three different influent conditions (BC1, AC1, AC2). nirS, nosZ, AOB, and NOB population densities were presented across the bioreactors from the highest to the lowest ratio, respectively. nirS represented the highest population density for both bioreactors. For BIPGEM, nirS population density increased with $1.89 \times 10^{+4}$, $8.48 \times 10^{+4}$, and $9.28 \times 10^{+5}$ (mol·g^{-1}) at BC1, AC1, and AC2, respectively. In contrast, nirS population density varied for ZIPGEM between $2.29 \times 10^{+5}$, $5.27 \times 10^{+3}$, and $7.05 \times 10^{+5}$ (mol·g^{-1}) at BC1, AC1, and AC2, respectively (Fig. 5). Similarly, nosZ population density followed the same pattern as nirS for both media with $6.23 \times 10^{+2}$, $1.96 \times 10^{+3}$, and $6.45 \times 10^{+3}$ (mol·g^{-1}) for BIPGEM and $1.25 \times 10^{+3}$, $4.67 \times 10^{+2}$, and $8.71 \times 10^{+3}$ (mol·g^{-1}) for ZIPGEM (Fig. 5) at BC1, AC1, and AC2, respectively.

At a lower ratio than with denitrifying bacteria, the bioreactors were constituted by nitrifying bacteria, such as AOB and NOB. AOB population density varied for BIPGEM between $9.76 \times 10^{+0}$, $3.25 \times 10^{+0}$, and $3.25 \times 10^{+1}$ (mol·g^{-1}) at BC1, AC1, and AC2, respectively, but it increased for ZIPGEM between $1.37 \times 10^{+0}$, $5.99 \times 10^{+0}$, and $1.25 \times 10^{+1}$ (mol·g^{-1}) at BC1, AC1, and AC2, respectively (Fig. 6). NOB represented the lowest population density for both bioreactors. NOB population density varied for BIPGEM between $2.44 \times 10^{+0}$, $1.50 \times 10^{+1}$,

Table 4
Total DON concentration for BIPGEM and ZIPGEM at three different influent conditions.

Influent Conditions	Total DON concentration (BIPGEM)			Total DON concentration (ZIPGEM)		
	Cinf (mg·L^{-1} as N)	Ceff (mg·L^{-1} as N)	Removal Efficiency (%)	Cinf (mg·L^{-1} as N)	Ceff (mg·L^{-1} as N)	Removal Efficiency (%)
BC1	0.407	0.447	0	0.524	0.646	−0.23
AC1	1.861	1.016	45.4	1.654	1.191	27.9
AC2	2.551	1.688	33.8	1.730	1.309	24.3

Table 5
Total nitrogen concentration for BIPGEM and ZIPGEM at three different influent conditions.

	BIPGEM			ZIPGEM		
Total Nitrogen	Cinf ($mg{\cdot}L^{-1}$ as N)	Ceff ($mg{\cdot}L^{-1}$ as N)	Removal Efficiency (%)	Cinf ($mg{\cdot}L^{-1}$ as N)	Ceff ($mg{\cdot}L^{-1}$ as N)	Removal Efficiency (%)
BC1	0.61	0.55	9.63	0.65	0.75	−15.62
AC1	2.26	1.21	46.34	2.17	1.40	35.68
AC2	2.96	1.93	34.83	2.08	1.47	29.32
Ammonia	Cinf ($mg{\cdot}L^{-1}$ as N)	Ceff ($mg{\cdot}L^{-1}$ as N)	Removal Efficiency (%)	Cinf ($mg{\cdot}L^{-1}$ as N)	Ceff ($mg{\cdot}L^{-1}$ as N)	Removal Efficiency (%)
BC1	0.13	0.01	86.66	0.03	0.00	70.33
AC1	0.05	0.01	80.00	0.19	0.01	93.01
AC2	0.04	0.02	58.74	0.05	0.01	75.30
Nitrate	Cinf ($mg{\cdot}L^{-1}$ as N)	Ceff ($mg{\cdot}L^{-1}$ as N)	Removal Efficiency (%)	Cinf ($mg{\cdot}L^{-1}$ as N)	Ceff ($mg{\cdot}L^{-1}$ as N)	Removal Efficiency (%)
BC1	0.41	0.38	7.01	0.42	0.41	3.52
AC1	1.52	0.80	47.18	1.57	0.85	45.94
AC2	1.56	0.98	37.23	1.32	0.63	51.73
Nitrite	Cinf ($mg{\cdot}L^{-1}$ as N)	Ceff ($mg{\cdot}L^{-1}$ as N)	Removal Efficiency (%)	Cinf ($mg{\cdot}L^{-1}$ as N)	Ceff ($mg{\cdot}L^{-1}$ as N)	Removal Efficiency (%)
BC1	0.01	0.01	−14.00	0.01	0.01	−9.61
AC1	0.02	0.01	14.75	0.01	0.01	8.77
AC2	0.07	0.02	68.44	0.02	0.01	2.56

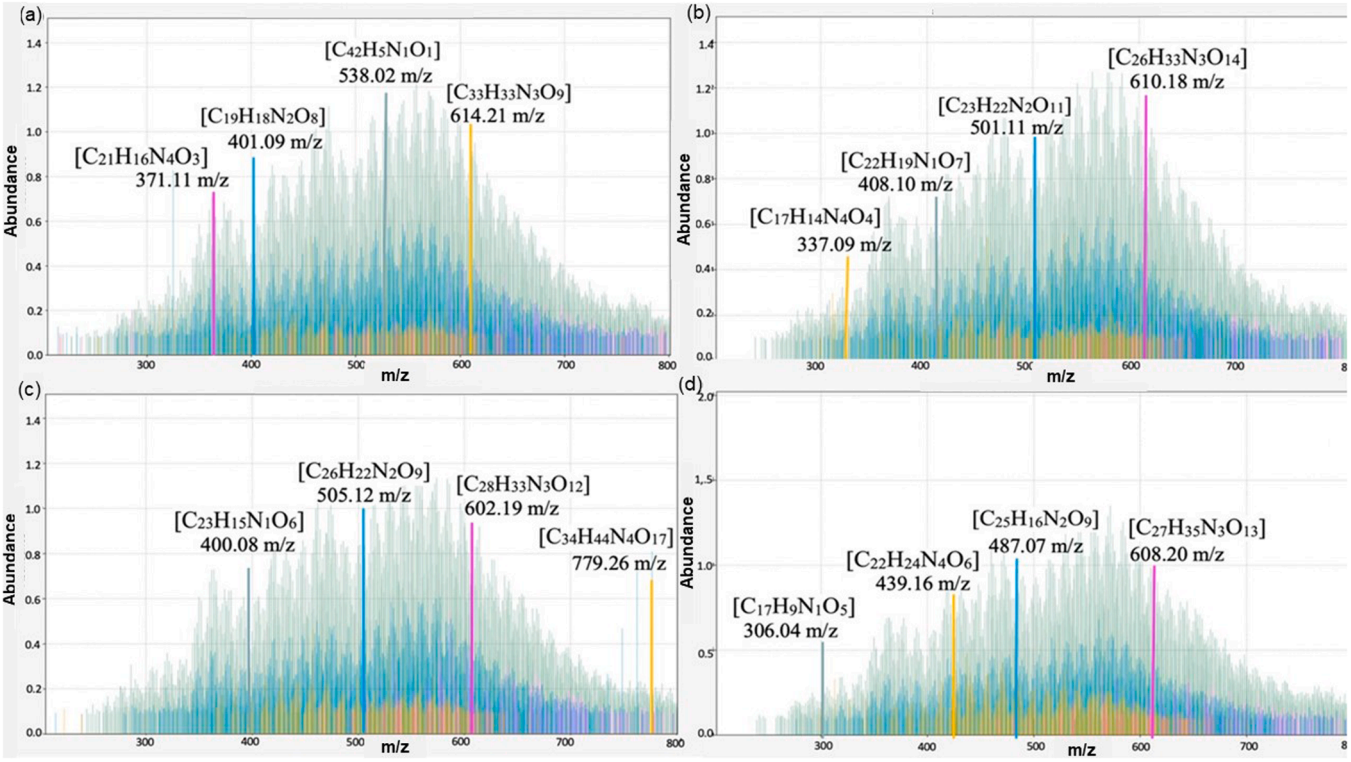

Fig. 7. 21 tesla (-) ESI FT-ICR MS analysis of DON in the effluents. (a) BIPGEM at AC1; (b) BIPGEM at AC2; (c) ZIPGEM at AC1; and (d) ZIPGEM at AC2 to show the difference of species distribution at the four conditions in the cascade filtration system.

and $1.37 \times 10^{+1}$ ($mol{\cdot}g^{-1}$) at BC1, AC1, and AC2, respectively, but it decreased for ZIPGEM between $2.36 \times 10^{+1}$, $1.04 \times 10^{+1}$, and $7.33 \times 10^{+0}$ ($mol{\cdot}g^{-1}$) at BC1, AC1, and AC2, respectively (Fig. 6).

3.4. Nitrogen removal efficiencies

The total DON concentrations from the influent and effluent were calculated through the ratios of total dissolved nitrogen and the dissolved inorganic nitrogen for both bioreactors at three different influent conditions. The total DON concentrations decreased in both media (Table 4) and BIPGEM can decompose more DON than ZIPGEM in the upflow cascade reactor. Total nitrogen and inorganic nitrogen, such as ammonia, nitrate, and nitrite, were collected and converted into units of nitrogen concentration. It shows that ammonia, nitrate, nitrite, and total nitrogen were removed from the stormwater runoff in both media for both bioreactors at three different influent conditions (Table 5). However, the removal efficiency of nitrite at AC2 in BIPGEM is much higher than that in ZIPGEM due to higher population density of NOB in BIPGEM (Fig. 6). But this is not the case of the removal efficiency of nitrate at AC2 in BIPGEM that is much lower than that in ZIPGEM due to lower population density of denitrifiers in BIPGEM. Moreover, the FT-ICR MS technique was performed to understand in detail to identify the relative abundance of DON per each heteroatom class and species.

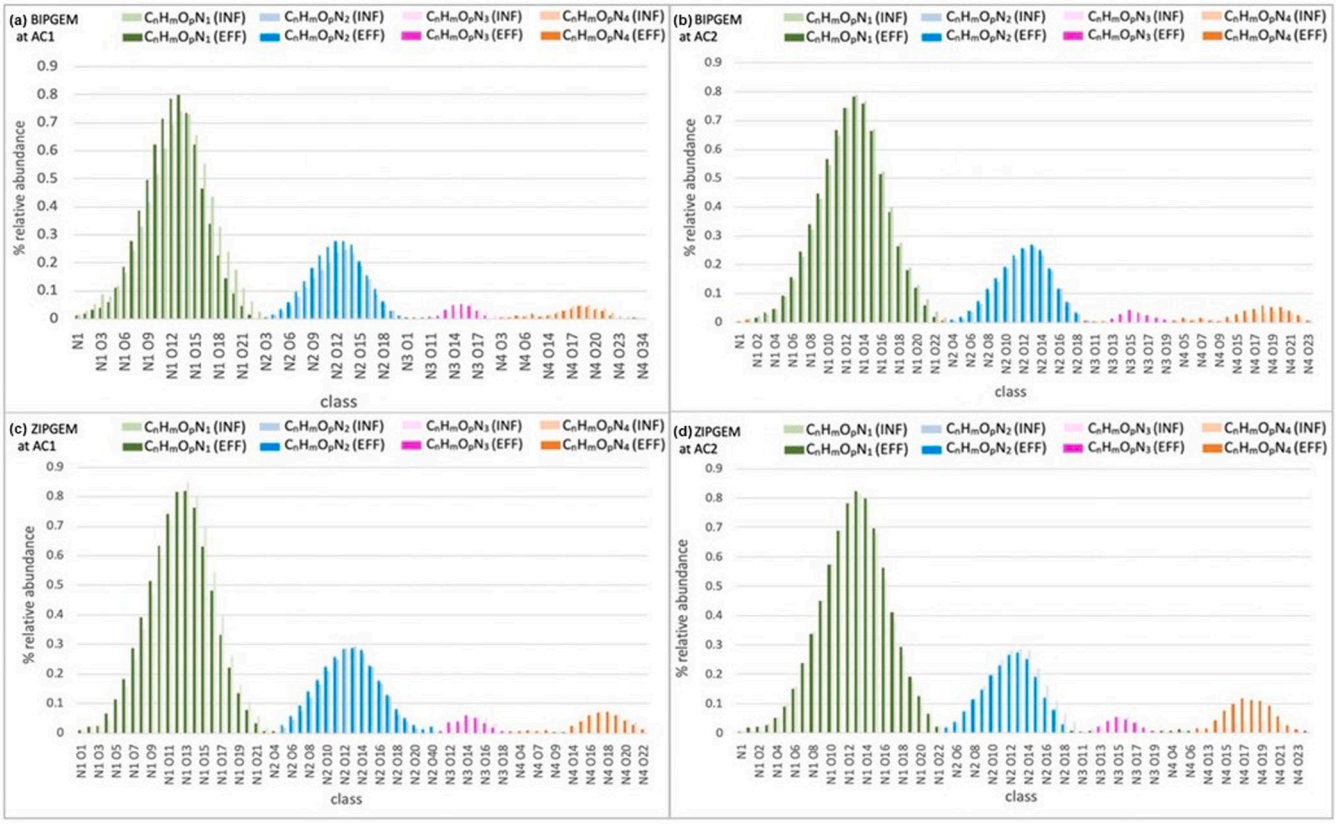

Fig. 8. Relative abundance of nitrogen heteroatom classes for influent and effluent samples. (a) BIPGEM at AC1 (after influent spiked with nitrate); (b) BIPGEM at AC2 (after influent spiked with nitrate and phosphate); (c) ZIPGEM at AC1; and (d) ZIPGEM at AC2.

Table 6a
The distribution of DON compounds in N1, N2, N3 and N4 heteroatom class in the influent and effluent of BIPGEM.

DON compounds	AC1 INF		AC1 EFF		AC2 INF		AC2 EFF	
	Number	Percentage (%)	Number	Percentage (%)	Amount	Percentage (%)	Number	Percentage (%)
$C_nH_mO_pN_1$	4491	62.06	3516	58.96	3433	64.51	3290	61.62
$C_nH_mO_pN_2$	1791	24.75	1800	30.19	1348	25.33	1378	25.81
$C_nH_mO_pN_3$	311	4.30	258	4.33	191	3.59	183	3.43
$C_nH_mO_pN_4$	632	8.73	389	6.52	350	6.58	488	9.14
Total	7236	100	5963	100	5322	100	5339	100

3.5. Abundance of DON heteroatoms

All data obtained in this study was ionized by the negative-ion electrospray (−ESI) from the FT-ICR MS. Therefore, there is a limitation for more complex heteroatoms class detention (Miranda et al., 2023). According to Bahureksa et al. (2021), FT-ICR MS achieves mass resolving power to identify a *m/z* difference of a single electron (Fig. 7). However, FT-ICR MS is not able to determine molecular structures, meaning that this data set is still a simple representation of DON (Bahureksa et al., 2021).

In this study, four DON heteroatom classes were recognized by −ESI (from N1 to N4) in a total of 64 to 74 peaks. DON classes for BIPGEM and ZIPGEM at AC1 and AC2 were illustrated in Fig. 8. Fig. 8a depicted a high relative abundance of DON heteroatom classes in the effluent for molecules with low atoms of oxygen. In contrast, there was a low abundance of DON heteroatom classes in the effluent for molecules rich in oxygen. At AC2, the relative abundance of N1, N2, and N3 heteroatom classes decreased, and the phosphate promoted a slight increase in the relative abundance of the N4 heteroatom class (Fig. 8b). ZIPGEM followed similar results to BIPGEM (Fig. 8c). However, in Fig. 8d ZIPGEM

Table 6b
The distribution of DON compounds in N1, N2, N3 and N4 heteroatom class in the influent and effluent of ZIPGEM.

DON compounds	AC1 INF		AC1 EFF		AC2 INF		AC2 EFF	
	Number	Percentage (%)	Number	Percentage (%)	Number	Percentage (%)	Number	Percentage (%)
$C_nH_mO_pN_1$	3267	58.66	3194	57.10	3336	59.50	3393	59.85
$C_nH_mO_pN_2$	1581	28.39	1724	30.82	1631	29.09	1338	23.60
$C_nH_mO_pN_3$	233	4.18	206	3.68	232	4.14	224	3.95
$C_nH_mO_pN_4$	488	8.76	470	8.40	408	7.28	714	12.59
Total	5569	100	5594	100	5607	100	5669	100

depicted a higher abundance of the DON N4 heteroatom class promoted by the nitrate and phosphate effect. These nutrients (nitrate and phosphate) worked as food sources for growing more complex nitrogen compounds with N4 heteroatoms, which was represented as carbohydrates in the Krevelen diagram.

To show the DON quality, the following Table 6 demonstrated the amount and percentage of N1, N2, N3, and N4 heteroatom class of BIPGEM (Table 6a) and ZIPGEM (Table 6b) at AC1 and AC2, respectively. After comparing the influents and effluents of BIPGEM (Table 6a), the number and percentage of $C_nH_mO_pN_1$ and $C_nH_mO_pN_3$ decreased in different degrees from influents to effluents (i.e., 4491 (62.06 %) of $C_nH_mO_pN_1$ in the influent at AC1 vs. 3516 (58.96 %) of $C_nH_mO_pN_1$ in the effluent at AC1; 191 (3.59 %) of $C_nH_mO_pN_3$ in the influent at AC2 vs. 183 (3.43 %) of $C_nH_mO_pN_1$ in the effluent at AC2. Such a decreasing trend on $C_nH_mO_pN_1$ and $C_nH_mO_pN_3$ also applied to ZIPGEM (Table 6b) at AC1 and AC2. For $C_nH_mO_pN_2$, both AC1 and AC2 experienced a mild increase of number from influents to effluents except for ZIPGEM at AC2 (i.e., 1791 (24.75 %) of $C_nH_mO_pN_2$ in BIPGEM's influent at AC1 vs. 1800 (30.19 %) of $C_nH_mO_pN_2$ in BIPGEM's effluent at AC1; 1581 (28.39 %) of $C_nH_mO_pN_2$ in ZIPGEM's influent at AC2 vs. 1724 (30.82 %) of $C_nH_mO_pN_2$ in ZIPGEM's effluent at AC2). Note that even though both BIPGEM (Table 6a) and ZIPGEM (Table 6b) experienced a mild decrease of $C_nH_mO_pN_4$ from the influent to the effluent at AC1, there was an increase of $C_nH_mO_pN_4$ from the influent to the effluent at AC2, given that the inclusion of phosphate promoted a slight increase in the relative abundance of the N4 heteroatom class due to the more intensive microbial activities. All original DON data are listed in the Excel table of the supplementary file 1.

3.6. Krevelen diagram

The relative abundance of species with the same $C_cH_hN_nO_oS_s$ was identified in the Kendrick mass scale (Wen et al., 2019). The Krevelen diagram contained data on ratios of hydrogen, carbon, and oxygen atoms (i.e., O/C and H/C; Valencia et al., 2020; Cheng et al., 2023). The molecules included in the Krevelen diagram were categorized as lipids with O/C = 0~0.3 and H/C = 1.5~2.2; proteins with O/C = 0.3~0.65 and H/C = 1.5~2.2; carbohydrates with O/C = 0.65~1.2 and H/C = 1.5~2.2; lignins with O/C = 0.1~0.65 and H/C = 0.7~1.7; tannins with O/C = 0.65~1.1 and H/C = 0.5~1.5; condensed aromatics with O/C = 0.1~1.2 and H/C = 0.1~0.7 (Xu et al., 2020); and unsaturated hydrocarbons with O/C = 0~0.1 and H/C = 0.7~1.5 (Wen et al., 2019; Valencia et al., 2020; Wang et al., 2022; Hu et al., 2020; Cheng et al., 2023). The molecules represented different biogeochemical mechanisms occurring in the bioreactors. Previous studies indicated that proteins, amino acid, and carbohydrates were products of microbial metabolism in association with intensive microbial interactions (Cheng et al., 2023; Sun et al., 2020; van Spanning et al., 2007; Valencia et al., 2020; Wu et al., 2018). Lignin compounds were derived from terrestrial soil organic matter in water (Xu et al., 2020). Oxygen also played an important role in understanding the bioreactor conditions that categorized the Krevelen diagrams in three zones according to Bahureksa et al. (2022). The molecules with an $O/C \leq 0.3$ ratio represented low relative abundance of oxygen. Molecules that were $0.3 < O/C \leq 0.6$ and $O/C > 0.6$ indicated mid-oxygen and high-oxygen levels, respectively. The target genes in this study indicated different metabolic pathways, where the denitrification respiration requires DON produced close to anaerobic conditions (van Spanning et al., 2007).

Rank analysis diagrams were produced from the analysis of intersample rankings attending up with four different datasets of samples associated with BIPGEM and ZIPGEM, respectively [see the supplementary file 2, Figure S1 (common pool of BIPGEM) and Figure S2 (common pool of ZIPGEM)]. For example, from the influent and effluent of BIPGEM at AC1, it is evidenced that the fourth rank was shifted with more oxygen components and components occupying the stoichiometric range from lignin-like compounds to tannin compounds based on the

Table 7a
Results of Inter Sample Rankings Analysis of Elemental Formula Compositions Intensities in BIPGEM.

Compounds	Sample	Intensity	Mass Peak Rank	Inter Sample Rank
$C_{42}H_{33}N_1O_{22}$	BIPGEM-AC1-INF	10,834,372.94	5718	3
	BIPGEM-AC1-EFF	14,427,753.15	5928	4
	BIPGEM -AC2-INF	11,956,073.10	5228	2
	BIPGEM -AC2-EFF	10,220,183.10	5097	1
$C_{33}H_{36}N_2O_{16}$	BIPGEM -AC1-INF	5179,076.06	3018	1
	BIPGEM -AC1-EFF	6902,420.43	4262	3
	BIPGEM -AC2-INF	9625,335.38	4865	4
	BIPGEM -AC2-EFF	7093,858.09	4234	2
$C_{33}H_{35}N_3O_{16}$	BIPGEM -AC1-INF	4678,543.69	2727	1
	BIPGEM -AC1-EFF	5890,483.51	3682	3
	BIPGEM -AC2-INF	5906,409.04	3576	2
	BIPGEM -AC2-EFF	6630,567.60	4026	4
$C_{31}H_{30}N_4O_8$	BIPGEM -AC1-INF	3068,191.22	1702	2
	BIPGEM -AC1-EFF	3753,573.87	2361	3
	BIPGEM -AC2-INF	2704,460.72	1635	1
	BIPGEM -AC2-EFF	6441,584.23	3939	4

Table 7b
Results of Inter Sample Rankings Analysis of Elemental Formula Compositions Intensities in ZIPGEM.

Compounds	Sample	Intensity	Mass Peak Rank	Inter Sample Rank
$C_{42}H_{45}N_1O_{19}$	ZIPGEM-AC1-INF	9662,008.90	5209	2
	ZIPGEM -AC1-EFF	8669,087.17	5105	1
	ZIPGEM -AC2-INF	11,101,636.17	5391	3
	ZIPGEM -AC2-EFF	12,957,359.17	5627	4
$C_{34}H_{34}N_2O_{16}$	ZIPGEM -AC1-INF	9418,376.47	5167	2
	ZIPGEM -AC1-EFF	6958,795.68	4487	1
	ZIPGEM -AC2-INF	9901,071.63	5189	3
	ZIPGEM -AC2-EFF	10,480,179.33	5346	4
$C_{30}H_{29}N_3O_{15}$	ZIPGEM -AC1-INF	3516,091.58	2197	2
	ZIPGEM -AC1-EFF	3545,263.64	2295	4
	ZIPGEM -AC2-INF	3532,598.64	2213	3
	ZIPGEM -AC2-EFF	3294,291.56	2091	1
$C_{28}H_{26}N_4O_7$	ZIPGEM -AC1-INF	1700,913.73	827	3
	ZIPGEM -AC1-EFF	1581,408.76	741	2
	ZIPGEM -AC2-INF	1385,249.97	561	1
	ZIPGEM -AC2-EFF	1901,286.19	974	4

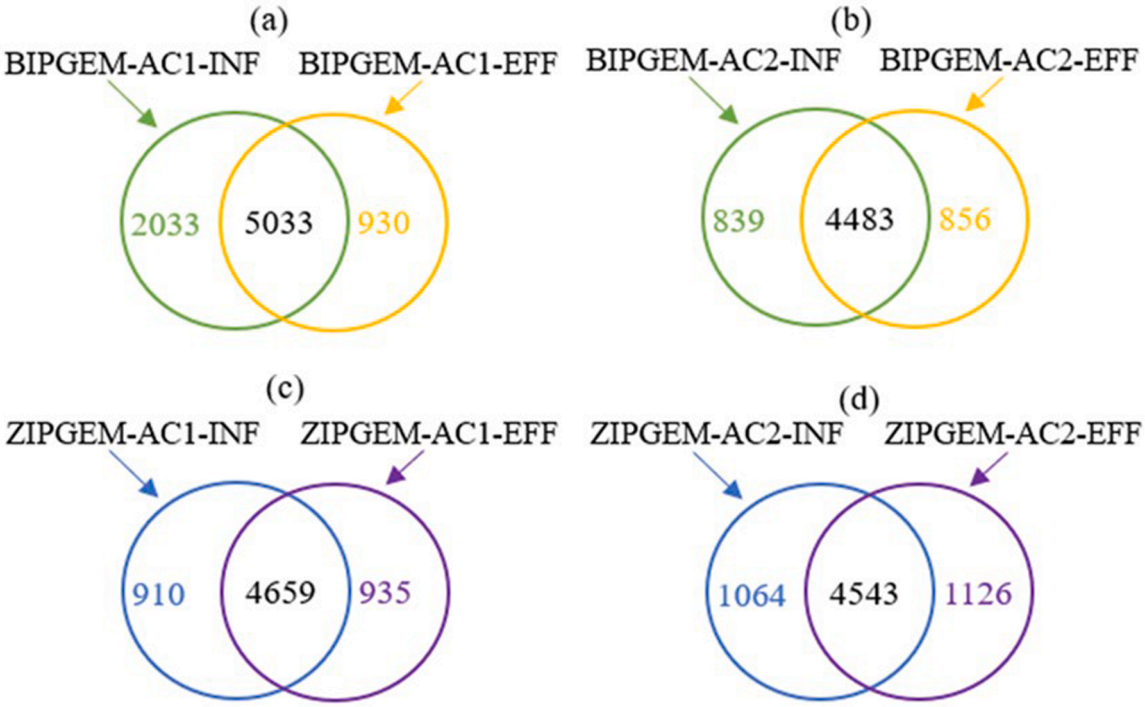

Fig. 9. The presence and absence diagrams of DON compounds in BIPGEM at (a) AC1 and (b) AC2 as well as ZIPGEM at (c) AC1 and (d) AC2.

influent [Figure S1(a)] and the effluent [Figure S1(b)]. However, at AC2, the fourth rank became more prevalent due to the presence of lignin-like compounds in the effluent than those in the influent. ZIPGEM has a similar change for the fourth rank as BIPGEM, while the third rank was more apparent in both influents of ZIPGEM than those of BIPGEM.

The inter-sample ranking technique (Tables 7a and 7b) and the presence / absence diagram (Fig. 9) were also prepared for summarizing DON quality changes (Herzsprung et al., 2012, 2017). A total of 5033 common components were found in the influent and effluent from BIPGEM at AC1, whereas a total of 4483 common components were found in the influent and effluent from BIPGEM at AC2. Component $C_{42}H_{33}N_1O_{22}$, for instance, received the 5097th rank in BIPGEM-AC2-EFF, the 5228th rank in BIPGEM-AC2-INF, the 5718th rank in BIPGEM-AC1-INF, and the 5928th rank in BIPGEM-AC1-EFF (Table 7a). For ZIPGEM, a total of 4659 common components were found at AC1, whereas a total of 4543 common components were found at AC2. $C_{42}H_{45}N_1O_{19}$, for instance, received the 5105th rank in ZIPGEM-AC1-EFF, the 5209th rank in ZIPGEM-AC1-INF, the 5391th rank in ZIPGEM -AC2-INF, and the 5627th rank in ZIPGEM -AC2-EFF (Table 7b).

The DON composition distribution of O/C and H/C ratios for BIPGEM and ZIPGEM at AC1 and AC2 were represented in Fig. 10. Overall, all effluent samples from Fig. 8 and Fig. 10 depicted an increase in complex compounds with the N4 class (orange) and a decrease in simple compounds with N1 (green), N2 (blue), and N3 (pink) classes. N1, N2, and N3 heteroatom classes included a low abundance of oxygen and were classified as condense aromatics and lignins. N4 classes were associated with carbohydrates. The reduction in DON was explained by the physical and chemical removal in the bioreactors (i.e., geotextile). In contrast, the rise in the N4 heteroatom class in carbohydrates occurred because of the increase of microbial metabolism (Wen et al., 2019; Valencia et al., 2020; Cheng et al., 2023), especially in ZIPGEM at AC2, which obtained the highest relative abundance of the N4 heteroatoms class.

Sun et al. (2020) and Mohan et al. (2016) investigated the relationship between metabolic pathways and bacteria with the N/C ratio. The relationship is given by the competitive growth between bacteria that use the C/N or N/C elements in a specific ratio. Nitrifiers have a slower growth rate under high C/N ratio conditions (Sun et al., 2020). Ling and Chen (2005) and Zhao et al. (2008) demonstrated a significant drop in the nitrification rate coinciding with a rise in the C/N ratio, particularly when it exceeded 1.11 (COD/N = 3). Consequently, a nitrification rate escalates with an increase in the N/C if N/C falls below 1. Bi et al. (2015) confirmed that a N/C ratio below 0.3 ensures a stable denitrification, capable of removing 70 % of TN. If the N/C ratio falls between 0.3 and 0.6 (0.67 in Mohanet al. 2016), an increase in N/C leads to a higher denitrification rate, potentially removing almost 95 % of TN. Fig. 11 plotted the diagrams of H/C against the N/C ratio. The diagrams were categorized and interpreted according to N/C ratios in previous studies and an N/C ratio below 0.3 stands for stable denitrification whereas an N/C ratio between 0.3 and 0.67 was represented as highly efficient denitrification (Mohan et al., 2016). In contrast, a higher N/C (0.67–1) could enhance the nitrification pathway that includes AOB and NOB (Carrera et al., 2004). The C/N ratio had a remarkable impact on the microbial structures, functions, and metabolic pathways (Sun et al., 2020). Therefore, Fig. 11 reflected a relative abundance of DON in the zones categorized by metabolic pathways, such as nitrification and denitrification. Although Fig. 11 was classified by a distinct process of the nitrogen cycle, DON from other sources is present in the diagram. Therefore, additional methods are suggested to incorporate better support in the statistical classification, such as analysis of variance (ANOVA), principal component analysis (PCA; Cheng et al., 2023), LEfSe analysis of microbial abundance, and PICRUSt analysis (Sun et al., 2020).

4. Effect of phosphate on nitrate removal efficiencies

To explore the phosphate effect on nitrate removal efficiencies and the denitrification process, a PCA test was conducted for both media under different nutrient influent concentrations (BC1, AC1, and AC2). According to Ehrlich and Newman (2008), inorganic phosphate is taken up by living organisms as a nutrient source. Phosphate is also an essential component of ATP (ATP is a biomolecule that stores the energy necessary for metabolic pathways). Thus, adding phosphate

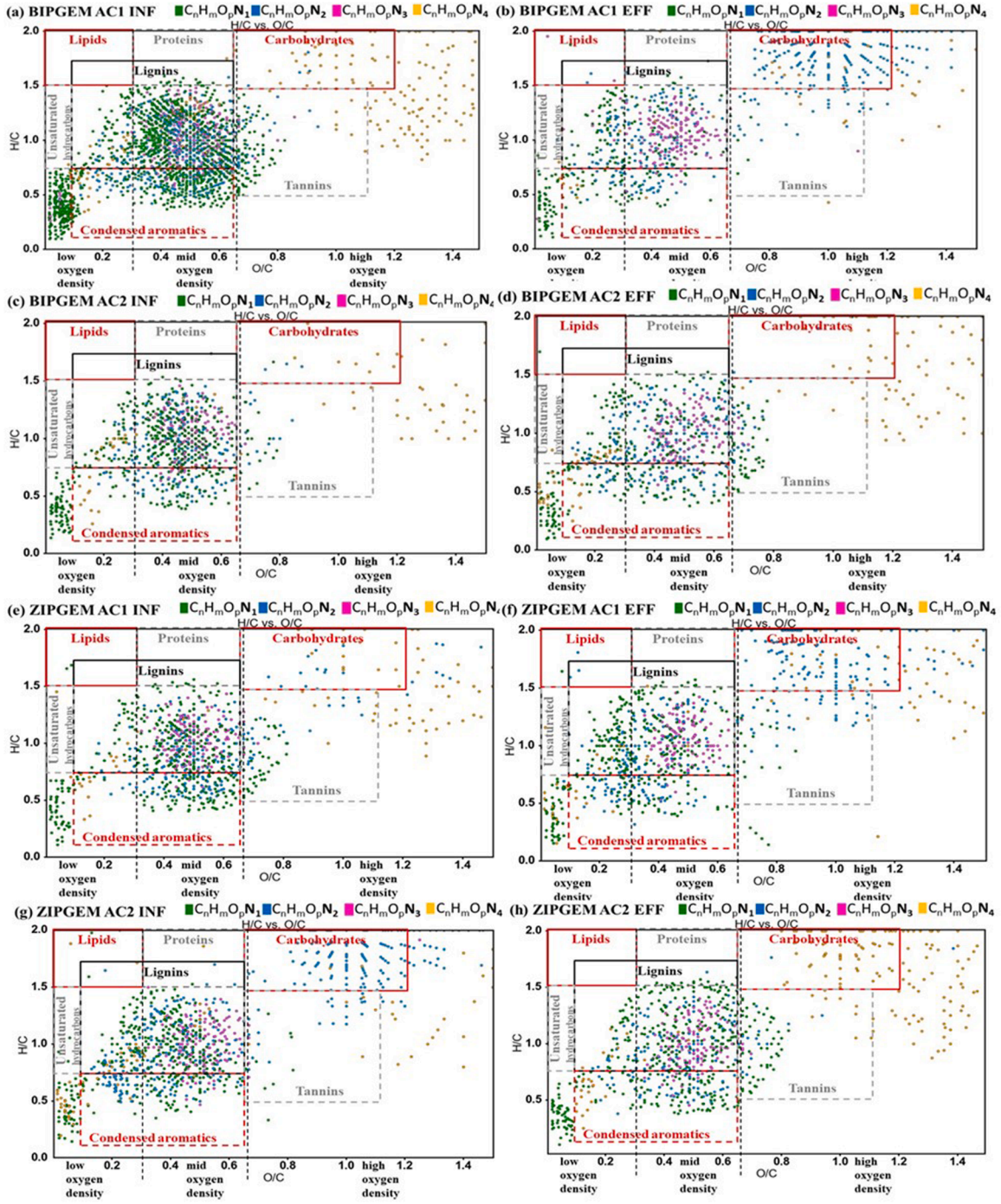

Fig. 10. Krevelen diagram for (a) influent BIPGEM at AC1, (b) effluent BIPGEM at AC1, (c) influent BIPGEM at AC2, (d) effluent BIPGEM at AC2, (e) influent ZIPGEM at AC1, (f) effluent ZIPGEM at AC1, (g) influent ZIPGEM at AC2, and (h) effluent ZIPGEM at AC2.

concentration in influents may help in increasing metabolic pathways and nitrate removal efficiencies in bioreactors. Additionally, including more nutrients in influents (i.e., phosphate and nitrate) may promote an increase in microbial activity. For instance, metabolic products of nitrate reducers are useful mechanisms of phosphate removal that include the reduction of iron in ferric phosphate to ferrous iron (Ehrlich and Newman, 2008). Fig. 12 depicts a direct relationship between denitrifiers, hydraulic retention time, nitrate and phosphate influent concentration, and nitrate removal efficiencies. 63 % and 30 % of PCA were detected for components in ZIPGEM and BIPGEM, respectively. Moreover, an opposite relationship was detected between silica and iron percentages in the samples (Table 3 and Fig. 12).

5. Linking don abundance with microbial population dynamics

According to Wen et al. (2019), the decomposition of DON is directly linked to ammonification, nitrification, and denitrification pathways driven by environmental factors such as biological disturbance, dissolved oxygen level, and carbon availability. Thus, DON composition and transformation is affected by microbial communities (Valencia et al., 2020). Two different pathways in the nitrogen cycle were depicted by the bioreactors. The nitrification pathway was analyzed via AOB and NOB (Fig. 6). The nitrification pathway enabled two reactions, ammonification by AOB and oxidation by NOB (Valencia et al., 2020; Madigan et al., 2021). In general, the low ratio in nitrifying bacteria was the result

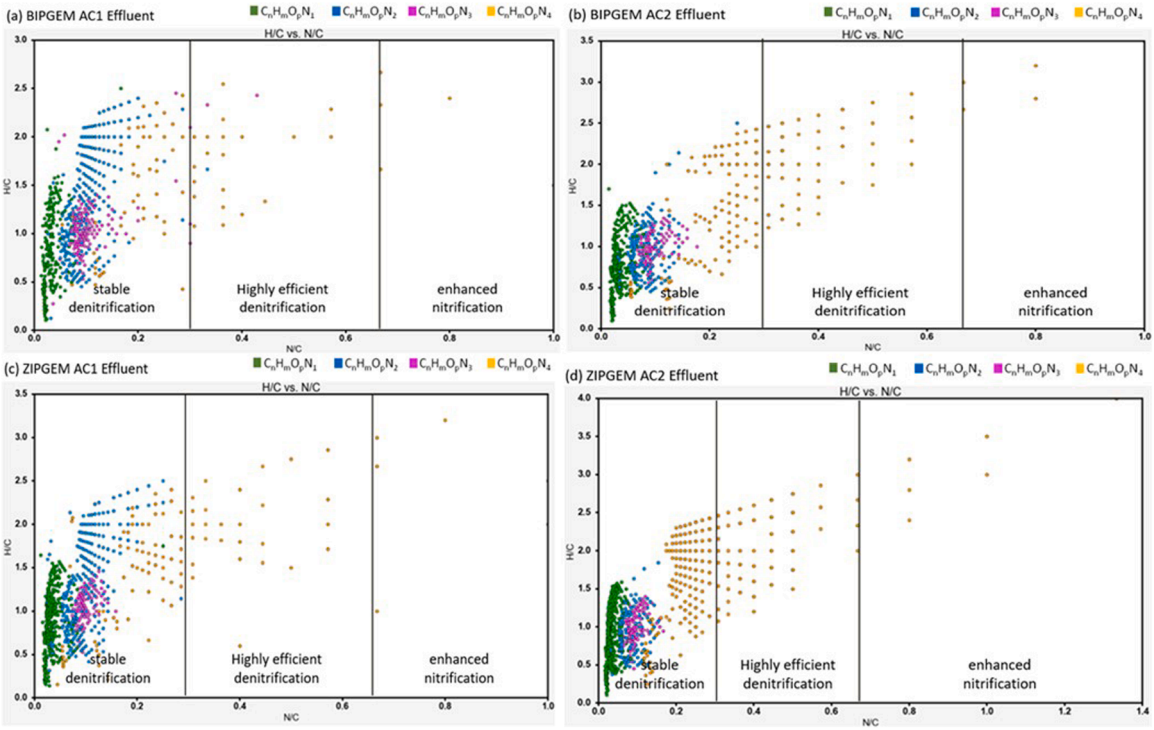

Fig. 11. Relation between N/C ratio diagrams with microbial metabolic pathways in the effluents of BIPGEM and ZIPGEM at AC1 and AC2. (a) BIPGEM at AC1, (b) BIPGEM at AC2, (c) ZIPGEM at AC1, and (d) ZIPGEM at AC2.

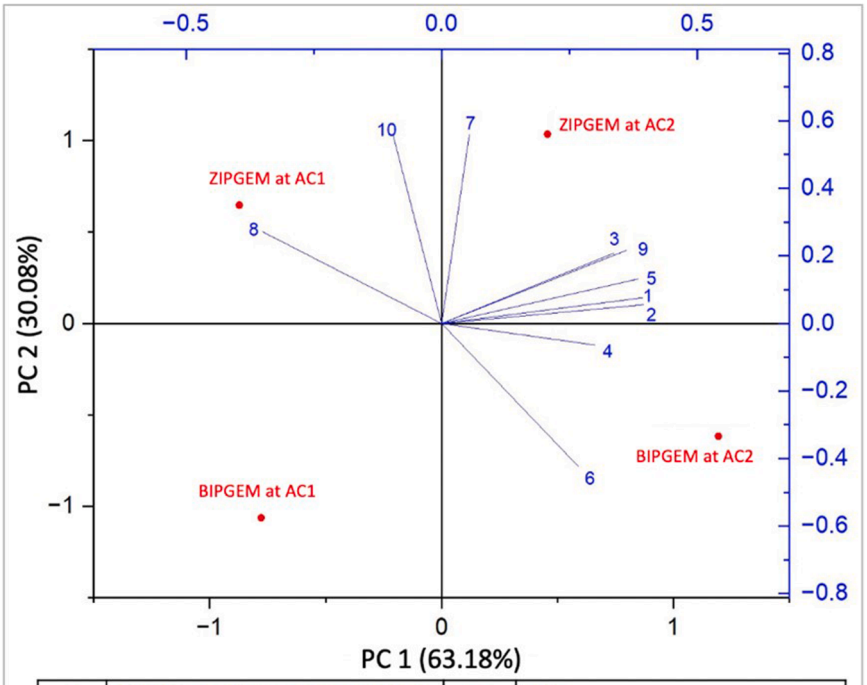

Fig. 12. Principal component analysis for performance assessment of BIPGEM and ZIPGEM.

of low oxygen in the media at AC1 and AC2 influent conditions. Between AOB and NOB, AOB represented a higher ratio of population density than NOB for both bioreactors. According to previous studies (Chang et al., 2010; Chang et al., 2018a; Crites and Tchobanoglous, 1998; Valencia et al. 2020), AOB converted ammonia (NH_3) to nitrite (NO_2^-), as evidenced by the decrease in ammonia concentration from influent to effluent (Table 5). In contrast, NOB consumed nitrite (NO_2^-) against nirS, and thus, NOB resulted in the lowest population densities in the bioreactors.

The denitrification pathway provided reduction reactions (Chang et al., 2010) from nitrate (NO_3^-) to nitrogen gas (N_2) and was analyzed via nirS and nosZ genes in both bioreactors. Because biochar in BIPGEM worked as a macronutrient source for denitrifying bacteria to grow, nirS and nosZ population densities in BIPGEM were more consistently growing up after spiking than those in ZIPGEM (Fig. 5). Furthermore, the biochar in BIPGEM promoted the production of nitrous oxide (N_2O) in the media, as evidenced by the higher ratio of nirS genes in BIPGEM than in ZIPGEM. Denitrification minimized the nitrogen load in stormwater runoff by removing the nitrate concentration. The addition of nitrate along with phosphate (AC1 and AC2) to the influent provided macronutrient sources for microorganisms to grow, which thrive living microorganisms in reductant environments in Stage 3. This effect was called anaerobic respiration when oxygen was substituted by electrons from any source (Madigan et al., 2021). Besides, relative abundance of DON increased in carbohydrates, which represented microbial metabolism. Therefore, the simultaneous presence of phosphate and nitrate in the influent increased not only nirS and nosZ population densities but also the abundance of DON for the N4 heteroatom class.

6. Conclusion

This study presents an integrative analysis of qPCR and FT-ICR MS that shows a unique linkage between pattern shifts of DON fractional removal and microbial species richness in a cascade upflow biofiltration process. It is indicative that the presence of biochar in BIPGEM promotes a higher population density of nirS and nosZ genes than in ZIPGEM. qPCR and DON analysis results indicated a low oxygen condition across both bioreactors at AC1 and AC2 influent conditions. Denitrifier bacteria were represented by nirS and nosZ population density, which was higher than AOB and NOB. For BIPGEM, nirS population density increased with $1.89 \times 10^{+4}$, $8.48 \times 10^{+4}$, and $9.28 \times 10^{+5}$ ($mol{\cdot}g^{-1}$) at BC1, AC1, and AC2, respectively. In contrast, nirS population density varied for ZIPGEM between $2.29 \times 10^{+5}$, $5.27 \times 10^{+3}$, and $7.05 \times 10^{+5}$ ($mol{\cdot}g^{-1}$) at BC1, AC1, and AC2, respectively. The results in qPCR were correlated with the relative abundance of nitrogen associated with carbohydrates which represented microbial metabolism and indicated more intensive microbial interactions. These interactions were also classified based on an N/C ratio, where DON with an N/C ratio > 0.2 represented nitrification (and > 0.33 represented denitrification). Moreover, the presence of phosphate and nitrate spiked in the influent increases the relative abundance of N4 atoms, especially in ZIPGEM. These N4 atoms are linked with carbohydrates, which implies more active metabolic pathways were promoted in the media matrix. All the findings herein are helpful for the balance among media characteristics, hydraulic loading rates, and physiochemical and microbiological reactions to achieve process reliability, sustainability, and resilience in future field applications.

CRediT authorship contribution statement

Alejandra Robles-Lecompte: Writing – original draft, Visualization, Investigation, Formal analysis, Data curation. **Jinxiang Cheng:** Writing – review & editing, Methodology, Investigation, Formal analysis, Data curation. **Amy M. McKenna:** Writing – review & editing, Visualization, Methodology, Data curation, Conceptualization. **Ni-Bin Chang:** Writing – review & editing, Writing – original draft, Supervision, Resources, Project administration, Methodology, Funding acquisition, Formal analysis, Conceptualization.

Declaration of competing interest

The authors declare that they have no known competing financial interests or personal relationships that could have appeared to influence the work reported in this paper.

Data availability

Data will be made available on request.

Acknowledgements

The authors acknowledge the financial support from the Shared Research Facilities fund at the University of Central Florida (16200710) and the Florida Department of Environmental Protection (Award ID: INV 008). A portion of this work was performed at the National High Magnetic Field Laboratory ICR User Facility, which is supported by the National Science Foundation Division of Chemistry and Division of Materials Research through DMR-2128556, (previous grant number DMR-1644779) and the State of Florida. The authors are thankful for the help from Andrea Valencia and Diana Ordonez during the experimental settings of this study.

Supplementary materials

Supplementary material associated with this article can be found, in the online version, at doi:10.1016/j.watres.2024.122130.

References

Azziz, G., Monza, J., Etchebehere, C., PJEjosb, Irisarri, 2017. nirS-and nirK-type denitrifier communities are differentially affected by soil type, rice cultivar and water management. 78, 20–28.

Bahureksa, W., Borch, T., Young, R.B., Weisbrod, C., Blakney, G.T., McKenna, A.M., 2022. Improved dynamic range, resolving power, and sensitivity achievable with FT-ICR mass spectrometry at 21 T reveals the hidden complexity of natural organic matter. Anal. Chem. 94 (32), 11382–11389.

Bahureksa, W., Tfaily, M.M., Boiteau, R.M., Young, R.B., Logan, M.N., McKenna, A.M., Borch, T., 2021. Soil organic matter characterization by Fourier transform ion cyclotron resonance mass spectrometry (FTICR MS): a critical review of sample preparation, analysis, and data interpretation. Environ. Sci. Technol. 55 ((14), 9637–9656.

Berman, T., Bronk, D.A., 2003. Dissolved organic nitrogen: a dynamic participant in aquatic ecosystems. Aquatic Microbial Ecol. 31 (3), 279–305.

Bi, Z., Takekawa, M., Park, M., Soda, G., Zhou, S., Qiao, J., Ike, M., 2015. Effects of the C/N ratio and bacterial populations on nitrogen removal in the simultaneous anammox and heterotrophic denitrification process: mathematic modeling and batch experiments. Chem. Eng. J. 280, 606–613.

Biosystems, A., 2015. Real-time PCR handbook. Life Thecnologies. Carlsbad, CA, USA.

Boldin, I.A., Nikolaev, E.N., 2011. Fourier transform ion cyclotron resonance cell with dynamic harmonization of the electric field in the whole volume by shaping of the excitation and detection electrode assembly. Rapid Commun. Mass Spectrom. 25 (1), 122–126.

Carrera, J., Vicent, T., Lafuente, J., 2004. Effect of influent COD/N ratio on biological nitrogen removal (BNR) from high-strength ammonium industrial wastewater. Process Biochemistry 39 (12), 2035–2041.

Crites, R., & Tchobanoglous, G. (1998). Small and decentralized wastewater management systems. *(No Title)*.

Chang, N.B., Wanielista, M., Daranpob, A., Xuan, Z., Hossain, F., 2010. New performance-based passive septic tank underground drainfield for nutrient and pathogen removal using sorption media. Environ. Eng. Sci. 27 (6), 469–482.

Chang, N.B., Wen, D., McKenna, A.M., Wanielista, M.P., 2018a. The impact of carbon source as electron donor on composition and concentration of dissolved organic nitrogen in biosorption activated media for stormwater and groundwater co-treatment. Environ. Sci. Technol. 52 (16), 9380–9390.

Chang, N.B., Wanielista, M., Singh, A., Duranceau, S.J., Wang, D., 2018b. Bio-sorption Activated Media For Nitrogen Removal In a Rapid Infiltration Basin–Monitoring Project. Florida Department of Environmental Protection, FL, USA.

Chang, N.B., Wen, D., Colona, B., Wanielista, M.P., 2019. Comparison of biological nutrient removal via two biosorption activated media between laboratory-scale and field-scale linear ditch for stormwater and groundwater co-treatment. Water. Air. Soil. Pollut. 230, 151.

Chen, T., Beu, S.C., Kaiser, N.K., Hendrickson, C.L., 2014. Note: optimized circuit for excitation and detection with one pair of electrodes for improved Fourier transform ion cyclotron resonance mass spectrometry. Rev. Sci. Instrum. 85 (6), 0666107/1-066107/3.
Cheng, H., Ma, S., Liao, K., Wang, J., Wu, B., Hu, H., Ren, H., 2023. Effect of external carbon source type on effluent dissolved organic nitrogen characteristics in postdenitrifying moving bed biofilm reactors: chemical molecular and microbial insights. Chem. Eng. J. 466, 143338.
Cooper, P., 2005. The performance of vertical flow constructed wetland systems with special reference to the significance of oxygen transfer and hydraulic loading rates. Water Sci. Technol. J. Int. Assoc. Water Pollut. Res. 51 (9), 81–90.
Corilo, Y.E., 2014. PetroOrg Software. Florida State University, Omics LLC: Tallahassee, Fl,.
Dewi, R., Agusnar, H., Alfian, Z., 2018. Characterization of technical kaolin using XRF, SEM, XRD, FTIR and its potentials as industrial raw materials. J. Phys.: Conference Series 1116 (4), 042010.
Dionisi, H.M., Layton, A.C., Harms, G., Gregory, I.R., Robinson, K.G., Sayler, G.S.J.A., et al., 2002. Quantification of Nitrosomonas oligotropha-like ammonia-oxidizing bacteria and Nitrospira spp. from full-scale wastewater treatment plants by competitive PCR. Appl. Environ. Microbiol. 68, 245–253.
Ehrlich, H.L., Newman, D.K., 2008. Geomicrobiology. CRC press, Boca Raton, FL, USA.
Emmett, M.R., White, F.M., Hendrickson, C.L., Shi, S.D.H., Marshall, A.G., 1998. Application of micro-electrospray liquid chromatography techniques to FT-ICR MS to enable high-sensitivity biological analysis. J. Am. Soc. Mass Spectrom. 9 (4), 333–340.
Gopal, G., Sankar, H., Natarajan, C., Mukherjee, A., 2020. Tetracycline removal using green synthesized bimetallic nZVI-Cu and bentonite supported green nZVI-Cu nanocomposite: a comparative study. J. Environmental. Management 254, 109812.
Griffiths, K.R., Burke, D.G., Emslie, K.R., 2011. Quantitative polymerase chain reaction: a framework for improving the quality of results and estimating uncertainty of measurement. Analytical Methods 3 (10), 2201–2211.
Hansell, D.A., Waterhouse, T.Y., 1997. Controls on the distributions of organic carbon and nitrogen in the eastern Pacific Ocean. Deep Sea Research Part I: Oceanographic Research Papers 44 (5), 843–857.
Hendrickson, C.L., Quinn, J.P., Kaiser, N.K., Smith, D.F., Blakney, G.T., Chen, T., Marshall, A.G., Weisbrod, C.R., Beu, S.C., 2015. 21 Tesla Fourier transform ion cyclotron resonance mass spectrometer: a national resource for ultrahigh resolution mass analysis. J. Am. Soc. Mass Spectrom. 26, 1626–1632.
Herzsprung, P., von Tümpling, W., Hertkorn, N., Harir, M., Büttner, O., Bravidor, J., Schmitt-Kopplin, P., 2012. Variations of DOM quality in inflows of a drinking water reservoir: linking of van Krevelen diagrams with EEMF spectra by rank correlation. Environ. Sci. Technol. 46 (10), 5511–5518.
Herzsprung, P., von Tümpling, W., Wendt-Potthoff, K., Hertkorn, N., Harir, M., Schmitt-Kopplin, P., Friese, K., 2017. High field FT-ICR mass spectrometry data sets enlighten qualitative DOM alteration in lake sediment porewater profiles. Org. Geochem. 108, 51–60.
Hu, H., Ma, S., Zhang, X., Ren, H., 2020. Characteristics of dissolved organic nitrogen in effluent from a biological nitrogen removal process using sludge alkaline fermentation liquid as an external carbon source. Water Res. 176, 115741.
Hughey, C.A., Hendrickson, C.L., Rodgers, R.P., Marshall, A.G., Qian, K., Kendrick, 2001. Mass Defect Spectroscopy: a Compact Visual Analysis for Ultrahigh-Resolution Broadband Mass Spectra. Anal. Chem. 73, 4676–4681.
Kaiser, N.K., McKenna, A.M., Savory, J.J., Hendrickson, C.L., Marshall, A.G., 2013. Tailored ion radius distribution for increased dynamic range in FT-ICR mass analysis of complex mixtures. Anal. Chem. 85 (1), 265–272.
Kloos, K., Mergel, A., Rösch, C., Bothe, H., 2001. Denitrification within the genus Azospirillum and other associative bacteria. Funct. Plant Biol. 28 (9), 991–998.
Krevelen, V.A.N., 1950. Graphical-statistical method for the study of structure and reaction processes of coal. Fuel 29, 269–284.
Kendrick, E., 1963. A mass scale based on $CH_2 = 14.0000$ for high resolution mass spectrometry of organic compounds. Anal. Chem. 35 (13), 2146–2154.
Kilgus-Vesely, S., 2023. Comparing Phosphorus Removal Efficiencies and Mechanisms via Two Cost-Effective Specialty Adsorbents in a Cascade Upflow Filtration System. Honors Undergrad. Theses. Jan. 2023[Online]. Available: https://stars.library.ucf.edu/honorstheses/1369.
Lahin, F.A., Sarbatly, R., Chel-Ken, C., 2021. Point-of-use upflow sand filter for rural water treatment using natural local sand: understanding and predicting pressure drop. IOP Conf. Ser. Mater. Sci. Eng. 1192 (1), 012008 https://doi.org/10.1088/1757-899X/1192/1/012008. Nov. 2021.
Libby, P.S., Wheeler, P.A., 1997. Particulate and dissolved organic nitrogen in the central and eastern equatorial Pacific. Deep Sea Research Part I: Oceanographic Research Papers 44 (2), 345–361.
Ling, J., Chen, S., 2005. Impact of organic carbon on nitrification performance of different biofilters. Aquac. Eng. 33 (2), 150–162.
Liu, Y., Cao, X., Yu, Z., Song, X., Qiu, L., 2016. Controlling harmful algae blooms using aluminum-modified clay. Mar. Pollut. Bull. 103 (1–2), 211–219.
Madigan, M.T., Bender, K.S., Buckley, D.H., Sattley, W.M., Stahl, D.A., 2021. Ecological Diversity of Bacteria. Brock Biology of Microorganisms, 16th Edition. Pearson, Hoboken, NJ, USA, pp. 478–518.
Miranda, C., Boiteau, R.M., McKenna, A.M., Knapp, A.N., 2023. Quantitative and qualitative comparison of marine dissolved organic nitrogen recovery using solid phase extraction. Limnol. Oceanography: Methods. https://doi.org/10.1002/lom3.10558.
Mishra, S.P., Sarkar, U., Taraphder, S., Datta, S., Swain, D., Saikhom, R., Laishram, M., 2017. Multivariate statistical data analysis-principal component analysis (PCA). Int. J. Livestock Research 7 (5), 60–78.
Mohan, T.K., Nancharaiah, Y.V., Venugopalan, V.P., Sai, P.S., 2016. Effect of C/N ratio on denitrification of high-strength nitrate wastewater in anoxic granular sludge sequencing batch reactors. Ecol Eng 91, 441–448.
Ordonez, D., Valencia, A., Chang, N.B., Wanielista, M.P., 2020a. Synergistic effects of aluminum/iron oxides and clay minerals on nutrient removal and recovery in water filtration media. J. Clean. Prod. 275, 122728.
Ordonez, D., Valencia, A., Elhakiem, H., Chang, N.B., Wanielista, M.P., 2020b. Adsorption thermodynamics and kinetics of Advanced Green Environmental Media (AGEM) for nutrient removal and recovery in agricultural discharge and stormwater runoff. Environ. Pollut. 266, 115172–115172.
Ordonez, D., Valencia, A., Pereira, B., Chang, N.B., 2022. Color removal for large-scale interbasin water transfer: experimental comparison of five sorption media. Environ. Res. 212, 113208.
Plessl, K., Russ, A., Vollprecht, D., 2023. Application and development of zero-valent iron (ZVI) for groundwater and wastewater treatment. Int. J. Environ. Sci. Technol. 20 (6), 6913–6928.
Raimbault, P., Slawyk, G., Boudjellal, B., Coatanoan, C., Conan, P., Coste, B., Pujo-Pay, M., 1999. Carbon and nitrogen uptake and export in the equatorial Pacific at 150 W: evidence of an efficient regenerated production cycle. J. Geophysical Research: Oceans 104 (C2), 3341–3356.
Rotthauwe, J.H., Witzel, K.P., Liesack, W., 1997. The ammonia monooxygenase structural gene amoA as a functional marker: molecular fine-scale analysis of natural ammonia-oxidizing populations. Appl. Environ. Microbiol. 63 (12), 4704–4712.
Savory, J.J., Kaiser, N.K., McKenna, A.M., Xian, F., Blakney, G.T., Rodgers, R.P., Hendrickson, C.L., Marshall, A.G., 2011. Fourier transform ion cyclotron resonance mass measurement accuracy with a "Walking" calibration equation. Anal. Chem. 83 (5), 1732–1736.
Scientific, T.F., 2014. Real-time PCR handbook.
Shrestha, P., Hurley, S.E., Wemple, B.C., 2018. Effects of different soil media, vegetation, and hydrologic treatments on nutrient and sediment removal in roadside bioretention systems. Ecol Eng 112, 116–131.
Smith, D.F., Podgorski, D.C., Rodgers, R.P., Blakney, G.T., Hendrickson, C.L., 2018. 21 Tesla FT-ICR mass spectrometer for ultrhigh resolution analysis of complex organic mixtures. Anal. Chem. 90 (3), 2041–2047.
Sun, H., Shi, W., Cai, C., Ge, S., Ma, B., Li, X., Ding, J., 2020. Responses of microbial structures, functions, metabolic pathways and community interactions to different C/N ratios in aerobic nitrification. Bioresour. Technol. 311, 123422.
Tian, Huang, C., Wang, P., Wei, J., Li, X., Zhang, R., Ling, D., Feng, C., Liu, H., Wang, M., Liu, Z, 2023. Enhanced elimination of Cr(VI) from aqueous media by polyethyleneimine modified corn straw biochar supported sulfide nanoscale zero valent iron: performance and mechanism. Bioresour. Technol. 369, 128452–128452.
Valencia, A., Ordonez, D., Wen, D., McKenna, A.M., Chang, N.B., Wanielista, M.P., 2020. The interaction of dissolved organic nitrogen removal and microbial abundance in iron-filings based green environmental media for stormwater treatment. Environ. Res. 188, 109815.
van Spanning, R.J., Richardson, D.J., Ferguson, S.J., 2007. Introduction to the biochemistry and molecular biology of denitrification. Biology of the Nitrogen Cycle. Elsevier, Amsterdam, the Netherlands, pp. 3–20.
Wang, J., Zheng, F., Yu, Z., Chen, J., Lu, H., 2022. Dissolved organic nitrogen derived from wastewater denitrification: composition and nitrogenous disinfection byproduct formation. J. Hazard. Mater. 440, 129775.
Wen, D., Chang, N.B., Wanielista, M., 2018. Comparative copper toxicity impact and enzymatic cascade effect on biosorption activated media and woodchips for nutrient removal in stormwater treatment. Chemosphere 213, 403–413.
Wen, D., Ordonez, D., McKenna, A., Chang, N.B, 2019. Fate and transport processes of nitrogen in biosorption activated media for stormwater treatment at varying field conditions of a roadside linear ditch. Environ. Res. 181, 108915.
Wen, D., Chang, N.B., Wanielista, M.P., 2020a. Assessing nutrient removal in stormwater runoff for urban farming with iron filings-based green environmental media. Sci. Rep. 10 (1), 9379.
Wen, D., Valencia, A., Ordonez, D., Chang, N.B., Wanielista, W.P., 2020b. Comparative nitrogen removal via microbial ecology between soil and green sorption media in a rapid infiltration basin for co-disposal of stormwater and wastewater. Environ. Res. 184, 109338.
Wu, X., Wu, L., Liu, Y., Zhang, P., Li, Q., Zhou, J., Chakraborty, R., 2018. Microbial interactions with dissolved organic matter drive carbon dynamics and community succession. Front. Microbiol. 9, 1234.
Xian, F., Hendrickson, C.L., Blakney, G.T., Beu, S.C., Marshall, A.G., 2010. Automated Broadband Phase Correction of Fourier Transform Ion Cyclotron Resonance Mass Spectra. Anal. Chem. 82 (21), 8807–8812.
Xu, H., Lin, C., Shen, Z., Gao, L., Lin, T., Tao, H., Lu, C., 2020. Molecular characteristics of dissolved organic nitrogen and its interaction with microbial communities in a prechlorinated raw water distribution system. Environ. Sci. Technol. 54 (3), 1484–1492.
Yang, Y., Sun, P., Padhye, L.P., Zhang, R., 2021. Photo-ammonification in surface water samples: mechanism and influencing factors. Sci. Total Environ. 759, 143547.
Zhao, C.H., Peng, Y.Z., Wang, S.Y., Tang, X.G., 2008. Influence of wastewater composition on biological nutrient removal in UniFed SBR process. Water Sci. Technology 58 (4), 803–810.

Zhang, Y., Zhang, R., Li, S.L., Mostofa, K.M., Fu, X., Ji, H., Sun, P., 2021. Photo-ammonification of low molecular weight dissolved organic nitrogen by direct and indirect photolysis. Sci. Total Environment 764, 142930.
Zheng, X., Wu, Q., Huang, C., Wang, P., Cheng, H., Sun, C., Zhu, J., Xu, H., Ouyang, K., Guo, J., Liu, Z., 2023. Synergistic effect and mechanism of Cd(II) and As(III) adsorption by biochar supported sulfide nanoscale zero-valent iron. Environ. Res. 231 (Pt 1), 116080–116080.
Zhu, F., Wu, Y., Liang, Y., Li, H., Liang, W., 2020. Degradation mechanism of norfloxacin in water using persulfate activated by BC@nZVI/Ni. Chemical Engineering J. 389, 124276.